

INFILTRATION AFFECTED  
BY FLOW OF AIR

by

David B. McWhorter

May 1971



HYDROLOGY PAPERS  
COLORADO STATE UNIVERSITY  
Fort Collins, Colorado

INFILTRATION AFFECTED BY FLOW OF AIR

by

David B. McWhorter

HYDROLOGY PAPERS

COLORADO STATE UNIVERSITY

FORT COLLINS, COLORADO 80521

May 1971

No. 49

#### ACKNOWLEDGEMENTS

This paper is based on the Ph.D. dissertation entitled "Infiltration Affected by Flow of Air" prepared by D.B. McWhorter. The author wishes to express his appreciation to the members of his graduate committee; Drs. S. Basri, D.K. Sunada, H.J. Morel-Seytoux and especially to Dr. A.T. Corey, for their guidance and suggestions throughout this study.

A special thanks is due to Mr. J.A. Brookman and Mr. H.R. Duke, both of whom contributed valuable time and ideas to this work.

Financial support for this study from the National Science Foundation through Grant G-2698 is gratefully acknowledged.

TABLE OF CONTENTS

	<u>Page</u>
Abstract . . . . .	viii
INTRODUCTION . . . . .	1
BACKGROUND . . . . .	2
Infiltration Equations . . . . .	2
Analyses Based on the Richards' Equation . . . . .	2
Two-Phase Flow Analyses . . . . .	3
THEORETICAL ANALYSIS . . . . .	4
Presentation of Equations for the Flow of Two Fluids in Porous Media . . . . .	4
Scaling the Flow Equations . . . . .	4
Similitude for Flow of Two Fluids in Porous Media . . . . .	5
Derivation of Differential Equation of Flow . . . . .	7
The Functions $f_w(\hat{S})$ , $E(\hat{S})$ , and $D(\hat{S})$ . . . . .	8
The Boundary and Initial Conditions for Imbibition Processes . . . . .	9
Solution for the Horizontal Case . . . . .	9
Solution for Horizontal Case in Terms of Fractional Flow Function . . . . .	10
Solution for the Vertical Case - Boundary Conditions I . . . . .	11
Solution for the Vertical Case - Boundary Conditions II . . . . .	13
Solution for the Vertical Case - Boundary Conditions III . . . . .	14
Solution for the Vertical Case - Boundary Conditions IV . . . . .	15
EXPERIMENTAL PROCEDURES . . . . .	17
Measurement of Hydraulic Properties . . . . .	17
Infiltration Subject to Boundary Conditions III . . . . .	18
Infiltration Subject to Boundary Conditions II and IV . . . . .	19
RESULTS AND DISCUSSION . . . . .	21
Imbibition in Semi-Infinite Media . . . . .	21
Infiltration in Finite Media . . . . .	25
Constant Rate Infiltration . . . . .	27
CONCLUSIONS AND RECOMMENDATIONS . . . . .	29
REFERENCES . . . . .	31
APPENDIX A . . . . .	33
APPENDIX B . . . . .	34
APPENDIX C . . . . .	35
APPENDIX D . . . . .	38
APPENDIX E . . . . .	39
APPENDIX F . . . . .	43

LIST OF TABLES

<u>Table</u>		<u>Page</u>
1	Observed Dependence of Ponding Time on Infiltration Rate . . . . .	28
A-1	Capillary Pressure - Relative Permeability - Saturation Data for Poudre Sand . . . . .	33
A-2	Relative Permeability - Saturation Data for Berea Sandstone - Imbibition . . . . .	33
A-3	Capillary Pressure - Saturation Data for Berea Sandstone . . . . .	33
B-1	Infiltration Data for Simulated Semi-Infinite Column of Poudre Sand . . . . .	34
B-2	Infiltration Data for Simulated Semi-Infinite Column of Berea Sandstone . . . . .	34
C-1	Infiltration Data for Column of Poudre Sand 990 cm Equivalent Length . . . . .	35
C-2	Infiltration Data for Colum of Poudre Sand 670 cm Equivalent Length . . . . .	35
C-3	Infiltration Data for Column of Poudre Sand 393 cm Equivalent Length . . . . .	36
C-4	Infiltration Data for Column of Poudre Sand 233 cm Equivalent Length . . . . .	36
C-5	Infiltration Data for Column of Poudre Sand 185 cm Equivalent Length . . . . .	37
C-6	Infiltration Data for Column of Berea Sandstone 17.4 cm Equivalent Length . . . . .	37
D-1	Air Pressure Build-up in Columns of Poudre Sand with Open Lower End . . . . .	38
E-1	Tap 1 - 2.30 cm From Source . . . . .	39
E-2	Tap 2 - 3.81 cm From Source . . . . .	39
E-3	Tap 3 - 5.32 cm From Source . . . . .	40
E-4	Tap 4 - 6.83 cm From Source . . . . .	40
E-5	Tap 5 - 8.55 cm From Source . . . . .	41
E-6	Tap 6 - 10.16 cm From Source . . . . .	41
E-7	Tap 7 - 11.76 cm From Source . . . . .	42
F-1	Physical Properties of Core Test Fluid . . . . .	43

LIST OF FIGURES

<u>Figure</u>		<u>Page</u>
1	Typical $f_w$ curve . . . . .	8
2	Typical curve showing the dependence of E and D on $\hat{S}$ . . . . .	8
3	Example curves showing the relationship between cumulative infiltration and time for various values of $\hat{P}_{af}$ . . . . .	16
4	Schematic diagram of Gamma-ray attenuation equipment . . . . .	17
5	Schematic diagram of equipment setup for constant rate experiments . . . . .	18
6	Typical curve showing the degree of homogeneity obtained in the Poudre sand columns . . . . .	19
7	Schematic diagram of equipment setup for infiltration experiments . . . . .	20
8	Example saturation profile for horizontal imbibition . . . . .	21
9	$F_{w1}$ and $f_w$ curves used for calculation of the profile in Figure 8 . . . . .	21
10	Comparison of theory and experiment for infiltration in Poudre Sand . . . . .	22
11	Relative permeability as a function of capillary pressure head for Poudre sand . . . . .	23
12	Capillary pressure head and relative permeability as functions of saturation for Poudre sand . . . . .	23
13	Relative permeability as a function of $\hat{S}$ for Poudre sand . . . . .	23
14	Capillary pressure head as a function of $\hat{S}$ for Poudre sand . . . . .	24
15	Air pressure head in columns of Poudre sand . . . . .	24
16	Comparison of theory and experiment for infiltration in Berea sandstone. . . . .	24
17	Relative permeability as a function of saturation for Berea sandstone. . . . .	24
18	Capillary pressure head as a function of saturation for Berea sandstone. . . . .	25
19	Comparison of theory and experiment for infiltration in finite columns of Poudre sand . . . . .	25
20	Infiltration in a column of Poudre sand - 990 cm equivalent length . . . . .	26
21	Infiltration in a column of Poudre sand - 670 cm equivalent length . . . . .	26
22	Infiltration in a column of Poudre sand - 393 cm equivalent length . . . . .	26
23	Infiltration in a column of Poudre sand - 233 cm equivalent length . . . . .	26
24	Infiltration in a column of Poudre sand - 185 cm equivalent length . . . . .	27
25	Infiltration in a column of Berea sandstone - 17.4 cm equivalent length. . . . .	27
26	Capillary pressure head as a function of time and position during constant rate infiltration . . . . .	27
27	Calculated capillary pressure as a function of time at the surface . . . . .	28
28	Calculated relationship between infiltration rate and ponding time . . . . .	28
29	Measured capillary pressure profiles during constant rate infiltration . . . . .	28

LIST OF SYMBOLS

<u>Symbol</u>	<u>Definition</u>	<u>Dimensions</u>
D	A function of saturation defined by $-EP'_c$	none
E	A function of saturation defined by $k_{ra} f_w$	none
$f_w$	Fractional flow function for case of negligible capillary and gravitational forces	none
$F_{w1}$	Horizontal fractional flow function	none
$F_{w2}$	Vertical fractional flow function	none
$F_{w3}$	Fractional flow function for constant rate infiltration	none
g	Gravitational constant	L/T <sup>2</sup>
$k_{ra}$	Relative permeability to air	none
$k_{rw}$	Relative permeability to liquid	none
K	Absolute permeability of porous medium	L <sup>2</sup>
L	Depth to impermeable boundary	L
$L_o$	Scale factor for length	L
M	Molecular weight of gas	M
$P_a$	Pressure of air	F/L <sup>2</sup>
$P_c$	Capillary pressure = $P_a - P_w$	F/L <sup>2</sup>
$P_d$	Capillary pressure at which air phase becomes discontinuous in the imbibition process	F/L <sup>2</sup>
$P_o$	Scale factor for pressure - Also pressure in liquid at $z=0$	F/L <sup>2</sup>
$P_w$	Liquid pressure	F/L <sup>2</sup>
$q_a$	Volume flux of air	L/T
$q_o$	Scale factor for volume flux	L/T
$q_w$	Volume flux of liquid	L/T
Q	Cumulative infiltration per unit of area	L
S	Liquid saturation	none
$S_i$	Initial saturation	none
$S_o$	Maximum saturation obtained in the imbibition process - Also, saturation at $z=0$ in constant rate infiltration	none
$\hat{S}$	Normalized saturation = $\frac{S-S_i}{S_o-S_i}$	none
t	Time	T
$t_o$	Scale factor for time	T
V	Total velocity = $q_a + q_w$	L/T
$V_i$	Volume of air in finite column of porous media	L <sup>3</sup>
x	Coordinate in horizontal flow case	L
z	Vertical coordinate	L

LIST OF SYMBOLS (cont.)

<u>Symbol</u>	<u>Definition</u>	<u>Deminsions</u>
$\alpha$	Constant of integration	none
$\beta$	Constant of integration	none
$\phi$	Porosity	none
$\psi$	The Boltzman variable = $\hat{x} \hat{t}^{-1/2}$	none
$\bar{\psi}$	Constant defined by equation (60)	none
$\mu_a$	Dynamic viscosity of air	F-T/L <sup>2</sup>
$\mu_w$	Dynamic viscosity of liquid	F-T/L <sup>2</sup>
$\rho_a$	Density of air	M/L <sup>3</sup>
$\rho_w$	Density of liquid	M/L <sup>3</sup>
$\nabla$	Del operator	L <sup>-1</sup>
$\hat{\phantom{x}}$	Refers to scaled values of variables	-----

## ABSTRACT

The phenomenon of one-dimensional flow of two immiscible fluids in porous media is studied both theoretically and experimentally with particular emphasis on the infiltration problem. The theoretical work is based on a differential equation derived by combining Darcy's law for both fluids with the equation of mass conservation. Experiments used in the study were designed to simulate field situations in which the resistance to flow of the displaced air significantly affects the flow of the liquid.

The first portion of the study is the determination of criteria for the construction of similar physical systems when the flow phenomenon is that of two-immiscible fluids, one of which is compressible. Five criteria for similitude are recognized and discussed. The analysis presented shows that the construction of rigorously similar physical systems, in this case, is impractical except in some simple cases in which an artificially induced body-force field can be induced.

A solution for the horizontal displacement of an incompressible non-wetting fluid by an incompressible wetting fluid under certain boundary conditions is derived. This solution is used as a starting point for the development of approximate analytical solutions for the vertical case. Predicted and experimental infiltration rates in Poudre sand agree quite well.

Both a theoretical and experimental analysis of infiltration, subject to a "rainfall" boundary condition are presented. The effect of counter-flowing air is included. The factors affecting the time at which ponding occurs are discussed. It is shown that the capillary pressure at the surface of the porous medium approaches the value at which ponding occurs almost asymptotically in time when the infiltration rate is near the unsaturated hydraulic conductivity. The surface value of capillary pressure (or saturation) at which ponding occurs is not the value predicted from a one-phase flow analysis.

Experiments on infiltration into bounded columns show that the rate of infiltration is significantly impeded by the compression of air in the closed column. The physics of this process is analyzed and discussed.

# INFILTRATION AFFECTED BY FLOW OF AIR

by

David B. McWhorter

## INTRODUCTION

The objectives of this study were two-fold:

- 1) To investigate the feasibility of constructing physical models to provide quantitative data applicable to prototype systems in which the flow phenomenon is that of two immiscible fluids, one of which is compressible.
- 2) To study the infiltration problem both theoretically and experimentally, by considering the problem as one of two-phase flow in a porous medium.

Laboratory experiments have been used extensively to study the flow of fluids in porous media. The objectives of the experiments often fall into one of two broad categories. The first category is concerned with the acquisition of basic and fundamental knowledge of the process. The concern of the second category is to provide data which can be used to design and predict the behavior of systems which cannot be conveniently tested in the laboratory. In the latter case, a method must be devised by which the differences in the physical and time scale between laboratory model and prototype are correctly taken into account. Usually, a solution to a mathematical model is the most desirable method for generalizing the results of such experiments. However, if the physical geometry and boundary conditions are sufficiently complicated, an analytical or numerical solution to the mathematical model may be impractical. In such a case, it is important to perform the experiments on a model which is physically similar in all important respects to the particular prototype in question. The results of the experiment can then be generalized to predict, quantitatively, the behavior of the prototype. The first objective of this study was to determine the criteria for the proper construction of such models.

To realize this objective, the appropriate governing equations were scaled according to the procedures used by Brooks and Corey (3), Scott and Corey (29), Corey et al. (8), and McWhorter and Corey (14). The work of these investigators has shown that selecting the appropriate system parameters as the scale factors for the variables is important if the maximum generalization and the least restrictive

criteria for similitude are to be obtained. The selection of the appropriate scaling parameters is discussed.

The second objective of this study falls into the first category discussed above. It was the intent to gain a further knowledge and understanding of two-phase flow in porous media with particular emphasis on the infiltration problem. Infiltration is the name given to the phenomenon of liquid in-take by porous materials. A quantitative description of infiltration is particularly important to scientists and engineers interested in the replenishment of soil water, ground water recharge, and infiltrating watersheds.

In the infiltration process, liquid enters the porous material under the influence of forces induced by gravity and capillarity. The occurrence of the phenomenon in the field always involves the displacement of air by water and is, therefore, a two-phase flow problem. Experimental and theoretical work have established that the infiltration rate is very large at small times and decreases to a limiting value at large times. High initial rates are the result of large forces induced by capillarity which rapidly decrease as the quantity of liquid in the porous material increases. As infiltration proceeds, the force induced by capillarity continues to be reduced, and ultimately the gravitational force becomes dominant.

Experimental and analytical methods were employed to attack the infiltration problem. The similarity transformation used by Philip to reduce the Richards' equation for horizontal flow to an ordinary differential equation was applied to the corresponding equations for two-phase flow. An approximate solution for vertical infiltration was derived. Experiments similar to those of Peck (17,18) were performed on columns of Poudre sand and Berea sandstone.

The problem of constant rate infiltration was also studied. Measurements of both the liquid and air pressure at various positions along the column as a function of time were made. An approximate solution for this case was derived. The solution elucidates the factors effecting the time at which ponding will occur.

## BACKGROUND

The literature concerning the infiltration of liquids in porous media is but a small portion of that on flow in porous media in general. Even so, the literature dealing directly with the infiltration phenomenon is quite extensive. The author has chosen to divide the discussion of the literature concerning infiltration into three broad categories: 1) infiltration equations, 2) analyses based on the Richards' equation, and 3) analyses based on the two-phase flow equations. Within this framework, significant experimental works are cited.

A large percentage of the previous work falls within the first two categories. Only in the past few years have investigators in the infiltration field addressed themselves to the studies indicated in the third category.

### Infiltration Equations

Early attempts to quantify the infiltration process were, for the most part, formulas which were obtained empirically or derived from a limited physical basis. The formula of Green and Ampt (11) was derived from a simplified model of the infiltration process. These authors assumed that the saturation profile propagates as a distinct front, behind which the saturation distribution was uniform at the maximum value obtainable in the imbibition process. It was assumed that the saturation of the porous material at points ahead of the advancing front remained at a uniform initial saturation. Combining Darcy's law and the continuity equation for this particular model results in a simple differential equation which is easily integrated to obtain:

$$\frac{Q}{C} - \frac{h_t \phi (S_0 - S_1)}{C} \ln \left( 1 + \frac{Q}{h_t \phi (S_0 - S_1)} \right) = t$$

where  $Q$  is the cumulative infiltration,  $\phi$  is the porosity,  $h_t$  is the total head  $S_0$  is the maximum saturation obtained on the imbibition cycle,  $S_1$  is the initial saturation,  $C$  is the hydraulic conductivity at  $S_0$ , and  $t$  is the time. The total head  $h_t$  is the sum of the capillary pressure head at the front and the depth of ponded liquid on the surface.

Another example is the formula of Horton (13):

$$f = f_e + (f_0 - f_e)e^{-\alpha t}$$

In this formula  $f$  is the infiltration rate at time  $t$ ,  $f_0$  is the initial infiltration rate,  $f_e$  is the limiting value of the infiltration rate, and  $\alpha$  is a constant with little or no physical interpretation. Childs (6) reports that this infiltration equation can best be regarded as an intuitive formula.

The above formulas are examples of algebraic equations derived from limited physical concepts. These equations are most often used by adjusting the parameters to fit a given set of data. In some cases, any physical significance of the various parameters is entirely lost. This is particularly true of the Green and Ampt formula.

Another infiltration formula commonly used is that proposed by Philip (22):

$$q_0 = \frac{S}{2} t^{-1/2} + B$$

Here  $q_0$  is the infiltration rate,  $t$  is time and  $S$  and  $B$  are constants which can be adjusted to give the best fit to measured infiltration rates. Philip proposed this equation after a detailed mathematical study of the physics of the infiltration process. This study will be discussed further in the next section.

The formulas given above do not constitute a complete list of such equations, but rather serve as examples of the work in this field.

### Analyses Based on the Richards' Equation

In 1931, Richards published a mathematical model of the capillary conduction of liquids in porous media. The equation (now known as the Richards' equation) has remained the basis for most of the work concerning infiltration since that time.

Richards combined Darcy's law and the equation of mass conservation for the liquid to obtain:

$$\frac{\partial}{\partial z} \left( C \frac{\partial h}{\partial z} \right) - \frac{\partial C}{\partial z} = \frac{\partial \theta}{\partial t}$$

In this equation,  $C$  is the hydraulic conductivity,  $\theta$  is the volumetric moisture content,  $h$  is the capillary suction head, and  $z$  and  $t$  are the space and time coordinates respectively.

The Richards' equation has been made more amenable to solution by converting it to an equation with  $\theta$  as the only dependent variable or to a form with  $h$  as the only dependent variable. The former is known as the "diffusivity" or water content form, and the latter is called the pressure head form. The conversion to either the water content or pressure head form is accomplished by the use of the functional relationships among  $C$ ,  $\theta$ , and  $h$ . The pressure head form is somewhat more general than the diffusivity form insofar as it can be applied in both saturated and unsaturated domains. The diffusivity form yields no information in saturated regions because the relationship between  $h$  and  $\theta$  is not single valued.

The series of papers (19 through 25) by Philip remains today as the classical analysis of infiltration. Philip obtained an approximate solution to the Richards' equation under the boundary conditions of constant water content at the upper surface and also for a ponded water boundary condition. The initial condition treated by Philip was a uniform water content. The equation for infiltration rate derived from this analysis is:

$$q_0 = \frac{S}{2} t^{-1/2} + (C_n + B) + \frac{3}{2} D t^{1/2} + 2 E t^{3/2} + \dots$$

A series of ordinary differential equations requiring numerical solution was presented from which each of the coefficients  $S$ ,  $B$ ,  $D$ ,  $E$  and etc. can be calculated. The constant  $C_n$  is the hydraulic conductivity associated with the initial water content.

The above series diverges for large  $t$ . Philip also proposed a large time approximation which can be used for values of  $t$  for which the above series diverges.

Parlange (16) recently proposed another approximate solution to the Richards' equation using an approach quite different from that of Philip. After transforming the diffusivity equation to an equation with  $z$  as the dependent variable, the unsteady term was neglected and a first approximation to the water-content profile was obtained by integration. Using this approximation, the unsteady term was calculated and reinserted in the differential equation. A second approximation was derived by again integrating the differential equation. Numerical agreement between the second approximation and the results of Philip's analysis was very good.

Parlange's method does not require numerical solution of ordinary differential equations, but does require considerable numerical integration. An advantage of Parlange's method is that the solution is valid for large times and the so-called profile at infinity evolves naturally from his approximations. This is true because the approximation makes use of the steady-state profile which becomes the proper profile at infinity as the infiltration rate approaches the unsaturated hydraulic conductivity.

Analytical work such as that done by Philip and Parlange has contributed immeasurably to the understanding of the physics of infiltration. It is unfortunate that such work is invariably limited to systems with simple initial and boundary conditions, simple geometries, and highly idealized media. Several investigators have used numerical techniques to solve these more difficult and more realistic problems. Among them are Hanks and Bowers (12), Rubin and Steinhart (28), Whisler and Klute (32,33), and Smith (31). Whisler and Klute, for example, studied infiltration into stratified soils under conditions of a non-uniform saturation distribution and included the effect of hysteresis in their calculations. Smith numerically solved the Richards' equation for conditions of stratified soil and included the effect of a time varying boundary condition.

#### Two-Phase Flow Analyses

It has long been recognized that infiltration is a process of two-phase flow even though most of the previous work has been based on a one-phase equation. Neglecting the resistance to flow of the air phase

has been justified by pointing to the small viscosity of air as compared to that of water. Free and Palmer (10) conducted experiments in 1940 which showed that infiltration was significantly effected when the air was not allowed to escape freely. In 1963, Wilson and Luthin (35) reported the results of experiments designed to show how air compression ahead of a wetting front affected the imbibition rate.

Youngs and Peck (36) discussed the effects of air compression on the imbibition rate from a physical point of view. Even though these authors mathematical analysis did not rigorously incorporate the effects of the air phase, their explanation of the physics of the phenomenon was quite detailed and did account for the effect of pore-air pressure in all important respects. Peck (17,18) reported experimental results of infiltration into bounded horizontal and vertical columns.

Adrian and Franzini (1) were able to account for (to some degree) the retarding effect of the compressed air. These authors' model was essentially that of Green and Ampt (11), except Adrian and Franzini included the resistance caused by the air phase. Similar work was done by Dicker (9).

Phuc (26) analyzed infiltration as a two-phase flow problem by solving the appropriate equations numerically. Phuc's model is capable of handling realistic hydrologic boundary conditions including those imposed by rainfall hyetographs. In addition, hysteresis and compressibility are incorporated in this model.

Brustkern and Morel-Seytoux (4) have used a unique approach to the solution of the governing two-phase flow equations. The method is principally analytic. To determine the shape of the saturation profile at any time, these authors neglected capillary pressure gradients which results in an equation for the saturation profile which contains a known function of saturation and the so-called total velocity. The total velocity is the algebraic sum of the flux of the liquid and air phases. The total velocity is calculated by integrating a form of Darcy's law (into which has been incorporated the flow of both phases) over the approximate profile determined in the previous time step. This integration is carried out giving full consideration to both capillary and gravity forces. Using this value of the total velocity, the profile for the next time step is calculated and the process is repeated. A significant aspect of these authors' work is that their solution is valid for large time as well as for small time.

The solution method derived by these authors is sufficiently general to handle flow problems in finite as well as semi-infinite media. To date, this appears to be the most promising model available for the solution of two-phase infiltration problems when the infiltration rate is of primary importance.

## THEORETICAL ANALYSIS

### Presentation of Equations for the Flow of Two Fluids in Porous Media

The equations which describe the flow phenomenon are based on the following assumptions:

- (1) Darcy's law is valid and can be applied equally well to either the wetting or non-wetting phase,
- (2) the physical properties of the porous medium are constant in time and space,
- (3) the porous medium is homogeneous and isotropic,
- (4) the two fluids are homogeneous and immiscible, and their viscosities are constant,
- (5) the wetting fluid is incompressible and the non-wetting fluid is compressible.

The foregoing assumptions allow one to write the following expressions:

$$\bar{q}_a = \frac{-Kk_{ra}}{\mu_a} (\nabla P_a + \rho_a \bar{g}) \quad (1)$$

$$\bar{q}_w = \frac{-Kk_{rw}}{\mu_w} (\nabla P_w + \rho_w \bar{g}) \quad (2)$$

$$\phi \frac{\partial S}{\partial t} + \nabla \cdot \bar{q}_w = 0 \quad (3)$$

and

$$-\phi \frac{\partial (\rho_a S)}{\partial t} + \nabla \cdot (\rho_a \bar{q}_a) = 0 \quad (4)$$

where,

- $\bar{g}$  = gravitational vector,
- $K$  = saturated permeability,
- $k_r$  = relative permeability - the ratio of the effective permeability to the saturated permeability,
- $P$  = pressure,
- $\bar{q}$  = volumetric flow rate per unit of area,
- $S$  = saturation of the wetting phase,
- $t$  = time
- $\phi$  = porosity,
- $\rho$  = density,
- $\mu$  = dynamic viscosity,

and the subscripts  $a$  and  $w$  refer to the non-wetting and the wetting fluids respectively. The pressures in equations (1) and (2) are measured relative to an absolute pressure of zero.

Equations (1) and (2) are Darcy's law written for the non-wetting and the wetting phases respectively. Equation (3) is the expression for mass conservation of the incompressible wetting fluid. The mathematical expression for mass conservation of the compressible non-wetting phase is given in equation (4).

The capillary pressure is defined as the difference between the non-wetting fluid pressure and the wetting-phase pressure; that is

$$P_c \equiv P_a - P_w \quad (5)$$

Additional independent relationships among the variables in the above equations are usually determined by experiment. These functional relationships are represented by the following equations:

$$\left. \begin{aligned} k_{ra} &= k_{ra}(S) \\ k_{rw} &= k_{rw}(S) \\ P_c &= P_c(S) \\ \rho_a &= \rho_a(P_a) \end{aligned} \right\} \quad (6)$$

The combination of equations (1) through (6) constitute a set of simultaneous equations which can be solved in principle when the appropriate initial and boundary conditions are specified.

### Scaling the Flow Equations

The principle objective of scaling the flow equations is to make the particular solution to the system of equations applicable to a larger class of problems than is the unscaled version. The numerical value of constants and constant coefficients in equations derived from physical principles almost always depends on the physical parameters of the problem. Unless all such constants and coefficients have the same value in two different situations, then the equations describing the two systems are different, even though the same physical phenomenon is occurring in both cases. In such a case, the solution obtained from one system is not applicable to the second one.

On the other hand, if by properly scaling the governing equations, all constants and coefficients can be reduced to constants that are independent of the physical parameters, then the solution obtained for one system can be applied to the second one by simply using the values of scale factors appropriate for the second system. Of course, it is not always possible to reduce all the constants and coefficients to constants independent of the system parameters. Usually, however, it is possible to reduce some of them and, thereby, gain some generality.

A scaling theory proposed by Brooks and Corey (3) has been found to yield criteria for similitude which are easily satisfied in practical situations when the process is one of drainage of the wetting phase. McWhorter and Corey (14) extended the theory to include two-phase drainage problems in which both fluids are incompressible. The following work makes use of the approach used by these investigators.

Each variable in the flow equations must be scaled by some characteristic parameter of the system. It is sufficient to designate these by:  $P_o$ ,  $t_o$ ,  $L_o$ ,  $\rho_o$  and  $q_o$ . The actual parameters to be used are selected so that the scaled equations provide a maximum generality and the criteria of similitude are the least restrictive.

Scaling equations (1) through (4) results in:

$$\frac{q_o \bar{q}_a \mu_a}{K} = -k_{ra} \left( \bar{\nabla} \frac{\hat{P}_a P_o}{L_o} + \rho_o \hat{\rho}_a \bar{g} \right) \quad (7)$$

$$\frac{q_o \hat{q}_w \mu_w}{K} = -k_{rw} (\hat{\nabla} \cdot \frac{P_w P_o}{L_o} + \rho_w \bar{g}) \quad (8)$$

$$\frac{\phi L_o}{t_o q_o} \frac{\partial S}{\partial t} + \hat{\nabla} \cdot \hat{q}_w = 0 \quad (9)$$

and

$$\frac{-\phi L_o}{t_o q_o} \frac{\partial (\rho_a S)}{\partial t} + \hat{\nabla} \cdot (\rho_a \hat{q}_a) = 0 \quad (10)$$

The symbol "hat" refers to the scaled form of the variables and operators.

Although the saturation  $S$  is already dimensionless, it is convenient to introduce the transformation:

$$\hat{S} = \frac{S - S_i}{S_o - S_i} \quad (11)$$

The significance of  $S_o$  and  $S_i$  depends upon whether the process is one of drainage or of wetting. In drainage processes it has been found that the criteria of similitude are made less restrictive by introducing equation (11) with  $S_o = 1.0$  and  $S_i$  equal to the residual saturation. In imbibition or wetting processes, the maximum saturation of the wetting phase is usually less than unity due to the entrapment of the non-wetting phase in the wetted zone.  $S_o$  is the symbol given the maximum saturation obtained in the imbibition process. The initial saturation is represented by  $S_i$ .

Using equation (11) in equations (9) and (10) yields:

$$\frac{\phi L_o (S_o - S_i)}{t_o q_o} \frac{\partial \hat{S}}{\partial t} + \hat{\nabla} \cdot \hat{q}_w = 0 \quad (12)$$

and

$$\frac{-\phi L_o (S_o - S_i)}{t_o q_o} \frac{\partial (\rho_a \hat{S})}{\partial t} + \hat{\nabla} \cdot (\rho_a \hat{q}_a) = 0 \quad (13)$$

It has been found by Brooks and Corey (3) that the following relationships among the scale factors are appropriate:

$$L_o = P_o / \rho_w g \quad (14)$$

$$q_o = K P_o / \mu_a L_o \quad (15)$$

$$t_o = \frac{L_o^2 \mu_a \phi (S_o - S_i)}{K P_o} \quad (16)$$

Substituting equations (14) through (16) into equations (7), (8), (12), and (13) results in:

$$\hat{q}_a = -k_{ra} (\hat{\nabla} \hat{P}_a + \hat{\rho}_a \bar{e}_3) \quad (17)$$

$$\hat{q}_w = \frac{-\mu_a}{\mu_w} k_{rw} (\hat{\nabla} \hat{P}_w + \bar{e}_3) \quad (18)$$

$$\frac{\partial \hat{S}}{\partial t} + \hat{\nabla} \cdot \hat{q}_w = 0 \quad (19)$$

$$\frac{-\partial (\hat{\rho}_a \hat{S})}{\partial t} + \hat{\nabla} \cdot (\hat{\rho}_a \hat{q}_a) = 0 \quad (20)$$

where the symbol  $\bar{e}_3$  is the unit vector parallel to the gravitational field. It should be noted that the constant density of the wetting fluid  $\rho_w$  has been selected as the scale factor for the variable  $\rho_a$ .

This selection was made because it automatically reduces the magnitude of the gravity term in equation (18) to unity. Therefore, the magnitude of this term no longer depends on any system parameter.

The equations (6) can be rewritten as scaled functions of the scaled variables:

$$\left. \begin{aligned} k_{ra} &= k_{ra}(\hat{S}) \\ k_{rw} &= k_{rw}(\hat{S}) \\ \hat{P}_c &= \hat{P}_c(\hat{S}) \\ \hat{\rho}_a &= \hat{\rho}_a(\hat{P}_a) \end{aligned} \right\} \quad (21)$$

#### Similitude for Flow of Two Fluids in Porous Media

The simultaneous solution of equations (17) through (21) will yield identical particular solutions for two different systems if the following conditions are satisfied. These conditions constitute criteria for similitude.

- (1) The overall geometry of the two systems must be such that corresponding dimensions form identical ratios to  $P_o / \rho_w g$ . This is accomplished if the systems are geometrically similar.
- (2) The theory implicitly requires the same orientation with respect to the gravitational field.
- (3) Initial and boundary conditions must be identical when expressed in terms of the scaled variables.
- (4) The viscosity ratio  $\mu_a / \mu_w$  must be identical in both systems.
- (5) The scaled functions represented by equations (21) must be identical.

Experimental results from physical models in which the flow is rigorously described by equations (17) through (21) represent particular solutions to these equations. Therefore, the five conditions listed above are conditions for the construction of similar physical systems as well as mathematical models. The ease with which the five criteria of similitude can be satisfied in practical situations, largely depends on the selection of  $P_o$ . Specifying  $P_o$  determines the remaining scale factors because of equations (14), (15), and (16). Before discussing the selection of  $P_o$  for imbibition processes, it is helpful to review the rationale used in the selection of  $P_o$  for drainage processes in which the non-wetting fluid can be considered incompressible. For this case, the density of the non-wetting phase  $\rho_a$  cancels in equation (20) and the last of equations (21) can be disregarded. Furthermore, the first three of equations (21) are given by well established empirical formulas. These are:

$$\left. \begin{aligned} k_{ra} &= (1-\hat{S})^2 (1-\hat{S}^{\frac{2+\lambda}{\lambda}}) \\ k_{rw} &= \hat{S}^{\frac{2+3\lambda}{\lambda}} \\ \hat{P}_c &= \hat{S}^{-1/\lambda}, \quad P_c \geq P_b \end{aligned} \right\} \quad (22)$$

In equation (22),  $\hat{S}$  is identical to the "effective saturation" as defined by Brooks and Corey (3). The symbol  $\lambda$  is the notation used by these authors to designate the pore-size distribution index. It is clear that, in any two systems for which  $\lambda$  has the same value, equations (22) will be identical for both systems. It is important to note, however, that the last of equations (22) can be written in that particular form only because the bubbling pressure  $P_b$  was selected as the scale factor for pressure. Examination of the unscaled relationship between  $P_c$  and  $S$ , that is,

$$P_c = P_b (\hat{S})^{-1/\lambda} \quad (23)$$

shows that any scale factor for pressure must be proportional to  $P_b$ ; otherwise the scaled relationship will not be identical, even in two systems with identical pore-size distributions. Since the bubbling pressures of the porous media in the two systems are usually different, the scale factor for pressure must be different in each case.

The important conclusion to be drawn is that the requirement that  $\hat{P}_c = \hat{P}_c(\hat{S})$  be identical in two similar systems governs the selection of  $P_o$  in each case. Unfortunately, explicit formulas analogous to equations (22) are not known for the imbibition process. Nevertheless, the above conclusion applies to imbibition processes as well as to drainage conditions.

Of particular interest in this study is the situation in which the non-wetting fluid is a gas. The last of equations (21) is the ideal gas law in this case:

$$\rho_a = \frac{P_o M}{\rho_o RT} P_a \quad (24)$$

where  $M$  is the molecular weight of the gas,  $R$  is the universal gas constant, and  $T$  is the absolute temperature. Condition 5 of the foregoing list implies that the coefficient  $P_o M / \rho_o RT$  must be identical in two similar systems.

The requirement that  $P_o M / \rho_o RT$  be identical in similar systems can be satisfied in several ways. The results must remain consistent with the conditions that  $\mu_a / \mu_w$  be equal to the corresponding quantity in the second system. Two of the various methods which can be used to meet the criteria of similitude are discussed in the following paragraphs.

Usually it is convenient to use the same two fluids in both systems. In such a case the scale factor  $P_o$  must be the same in order that the coefficient in equation (24) be the same value in each case. The requirement that  $P_o$  be the same in both systems conflicts with the requirement that  $\hat{P}_c = \hat{P}_c(\hat{S})$  be the same unless the same porous material is used. Using the same porous medium and the same fluids in both systems also insures that the first three of equations (21) are identical in the two situations.

The major disadvantage of using the same materials in both systems is that an artificial body-force field must be imposed on one system in order to gain a geometrical size reduction and a change in the time scale. This is true because of equation (14). It is conceivable that certain sufficiently simple prototype systems could be modeled in this way.

Practical prototype systems exist for which the construction of physical models in an artificially induced body-force field is not feasible. In this case, the ratio  $P_o / \rho_w$  must be different in the two systems. The requirement that  $P_o / \rho_w$  be different in turn implies that different gases must be used or that one system must be operated at a temperature different from the other. The latter possibility is impractical in view of the fact that the viscosity ratio  $\mu_a / \mu_w$  must remain identical in both systems. If different gases are used, the ratio of their molecular weights must be such that the coefficient in equation (24) is identical in both systems. Some difficulty in satisfying condition 4 can be anticipated because, for many gases, the viscosity is directly proportional to the molecular weight.

Even after the difficulties of using different fluids are overcome, there remains the problem of insuring that the first three of equations (21) are identical in both systems. When different fluids and different porous media are used, this is a formidable task.

The analysis presented in this section shows that the construction of similar physical systems in which the flow phenomenon is described by equations (1) through (6) is impractical except in some simple cases in which an artificial body-force field can be induced. Nevertheless, the scaled form of the equations and variables derived in this section are used throughout the remainder of this paper because of the economy in notation, and because analytical results will be directly applicable to a larger class of problems.

#### Derivation of Differential Equation of Flow

The differential equation is derived by combining the appropriate equations presented in the previous section. The coordinate system is selected so that the vertical coordinate  $z$  is positive downward. The volume flux of either phase is positive in the direction of increasing  $z$ . With this coordinate system and the assumption of incompressibility, the fundamental flow equations (17) through (20) reduce to:

$$\hat{q}_a = -k_{ra} \left( \frac{\partial \hat{p}_a}{\partial z} - \hat{\rho}_a \right) \quad (25)$$

$$\hat{q}_w = -\frac{\mu_a}{\mu_w} k_{rw} \left( \frac{\partial \hat{p}_w}{\partial z} - 1 \right) \quad (26)$$

$$\frac{\partial \hat{q}_w}{\partial z} = -\frac{\partial \hat{S}}{\partial t} \quad (27)$$

and

$$\frac{\partial \hat{q}_a}{\partial z} = \frac{\partial \hat{S}}{\partial t} \quad (28)$$

The definition of capillary pressure in scaled form is:

$$\hat{p}_c = \hat{p}_a - \hat{p}_w \quad (29)$$

Differentiating equation (29) with respect to  $\hat{z}$  gives:

$$\frac{\partial \hat{p}_c}{\partial z} = \frac{\partial \hat{p}_a}{\partial z} - \frac{\partial \hat{p}_w}{\partial z} \quad (30)$$

Solving equations (25) and (26) for the pressure gradients and substituting into equation (30) results in:

$$\frac{\partial \hat{p}_c}{\partial z} = \frac{\hat{q}_w}{k_{rw}} \frac{\mu_w}{\mu_a} - \frac{\hat{q}_a}{k_{ra}} - (1 - \hat{\rho}_a) \quad (31)$$

Subtracting  $\hat{q}_w/k_{ra}$  from both sides yields:

$$\frac{\partial \hat{p}_c}{\partial z} - \frac{\hat{q}_w}{k_{ra}} = \frac{\hat{q}_w \mu_w}{k_{rw} \mu_a} - \frac{(\hat{q}_w + \hat{q}_a)}{k_{ra}} - \Delta \hat{\rho} \quad (32)$$

where  $\Delta \hat{\rho} = 1 - \hat{\rho}_a$ .

A total velocity  $\hat{V}$  is defined as the sum of the flux vectors of each fluid,

$$\hat{V} \equiv \hat{q}_w + \hat{q}_a \quad (33)$$

Adding equations (27) and (28) shows that  $\hat{V}$  is independent of  $\hat{z}$  and, therefore, a function of time only.

Substituting equation (33) into equation (32), multiplying both sides by  $k_{ra}$  and solving for  $\hat{q}_w$  results in:

$$\hat{q}_w = \hat{V}(\hat{t}) \left( \frac{1}{1 + \frac{k_{ra} \mu_w}{k_{rw} \mu_a}} \right) + k_{ra} \left( \frac{1}{1 + \frac{k_{ra} \mu_w}{k_{rw} \mu_a}} \right) \left( \frac{\partial \hat{p}_c}{\partial z} + \Delta \hat{\rho} \right) \quad (34)$$

For incompressible fluids  $\Delta \hat{\rho}$  is a constant, and it is logical to redefine  $\hat{\rho}_o$  as  $\hat{\rho}_o = \rho_w - \rho_a$ . The constant  $\Delta \hat{\rho}$  becomes unity. The following definitions simplify the notation:

$$f_w(\hat{S}) \equiv \frac{1}{1 + \frac{k_{ra} \mu_w}{k_{rw} \mu_a}} \quad (35)$$

$$\text{and} \quad E(\hat{S}) \equiv k_{ra} f_w \quad (36)$$

Introducing equations (35) and (36) in equation (34) gives:

$$\hat{q}_w = \hat{V}(\hat{t}) f_w(\hat{S}) + E(\hat{S}) \frac{\partial \hat{p}_c}{\partial z} + E(\hat{S}) \quad (37)$$

Combining equation (37) with the mass conservation equation (equation (27)) yields:

$$\frac{\partial}{\partial z} \left\{ \hat{V}(\hat{t}) f_w + E \frac{\partial \hat{p}_c}{\partial z} + E \right\} = -\frac{\partial \hat{S}}{\partial t} \quad (38)$$

Equation (38) can be expressed with  $\hat{S}$  as the only dependent variable by substituting the following expressions:

$$\frac{\partial \hat{p}_c}{\partial z} = \hat{p}'_c \frac{\partial \hat{S}}{\partial z} \quad (39)$$

$$\frac{\partial E}{\partial z} = E' \frac{\partial \hat{S}}{\partial z} \quad (40)$$

and

$$\frac{\partial f_w}{\partial z} = f'_w \frac{\partial \hat{S}}{\partial z} \quad (41)$$

where the prime refers to the ordinary derivative with respect to  $\hat{S}$ . The result is:

$$\frac{\partial}{\partial z} \left( E \hat{p}'_c \frac{\partial \hat{S}}{\partial z} \right) + \left( \hat{V} f'_w + E' \right) \frac{\partial \hat{S}}{\partial z} = - \frac{\partial \hat{S}}{\partial t} \quad (42)$$

It is convenient to introduce the definition:

$$D(\hat{S}) = - E \hat{p}'_c \quad (43)$$

The negative sign is included in equation (43) to insure that  $D(\hat{S})$  is positive. Substitution of equation (43) into equation (42) results in the desired form of the differential equation:

$$\frac{\partial}{\partial z} D \frac{\partial \hat{S}}{\partial z} - \left( \hat{V} f'_w + E' \right) \frac{\partial \hat{S}}{\partial z} = \frac{\partial \hat{S}}{\partial t} \quad (44)$$

For completeness the relationships of the scaled variables to the unscaled variables are repeated here:

$$\hat{z} = z(\rho_w - \rho_a) g / p_o \quad (45)$$

$$\hat{p}_c = p_c / p_o \quad (46)$$

$$\hat{t} = \frac{K \left( (\rho_w - \rho_a) g \right)^2 t}{\mu_a p_o \phi (S_o - S_i)} \quad (47)$$

$$q = \frac{q_w}{K(\rho_w - \rho_a) g} \quad (48)$$

$$\hat{S} = \frac{S - S_i}{S_o - S_i}$$

The Functions  $f_w(\hat{S})$ ,  $E(\hat{S})$ , and  $D(\hat{S})$

From the definition of  $f_w(\hat{S})$ ,  $E(\hat{S})$ ,  $D(\hat{S})$  (equations (35), (36) and (43)), it is noted that for any particular soil and fluid system the functions are dependent only on saturation. This is because  $k_{ra}$ ,  $k_{rw}$ , and  $\hat{p}_c$  are functions of saturation only. It is pointed out in the section on similitude that the relationships  $k_{ra}(\hat{S})$ ,  $k_{rw}(\hat{S})$ , and  $\hat{p}_c(\hat{S})$  are obtained from experiment.

The function  $f_w$  has been called the fractional flow function in the petroleum industry. The name is derived because of its physical interpretation in situations where the gradients of capillary pressure and the influence of gravity are negligibly small. In this case,  $f_w$  can be interpreted as the ratio of the flux of the wetting phase  $q_w$  to the total velocity  $V$ . A typical example of  $f_w$  is shown in Figure 1. It is noted that  $f_w(1.0) = 1.0$  and that the curve approaches zero for small  $\hat{S}$ .

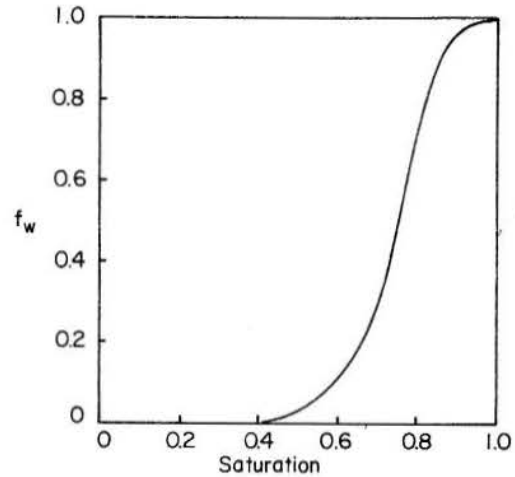


FIGURE 1 - Typical  $f_w$  curve.

The definition of  $E(\hat{S})$  shows the relationship between  $E$  and  $f_w$ . At small values of  $\hat{S}$ ,  $k_{ra} \approx 1.0$  and, therefore,  $E$  has about the same shape as  $f_w$  in the low saturation range. At large values of  $\hat{S}$ , near 1.0,  $k_{ra}$  approaches zero and, therefore,  $E$  exhibits a maximum and decreases to zero at  $\hat{S} = 1.0$ . A typical curve is shown in Figure 2.

The function  $D(\hat{S})$  plays a similar role in two-phase flow as the "diffusivity function" plays in one-phase flow. The two functions are quite dissimilar, however. It is noted in Figure 2 that  $D(\hat{S})$  is zero at both ends of the saturation scale and exhibits a maximum value at a saturation between zero and one.

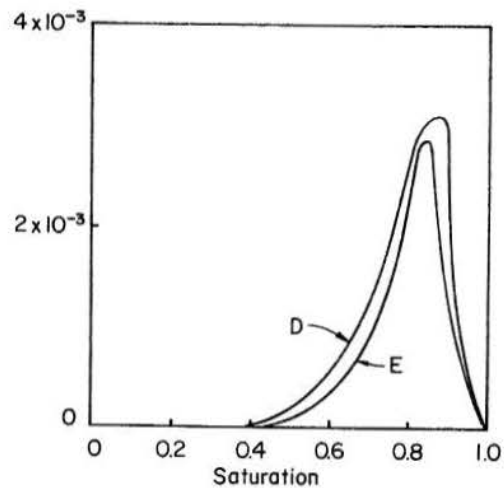


FIGURE 2 - Typical curve showing the dependence of  $E$  and  $D$  on  $\hat{S}$ .

The Boundary and Initial Conditions for Imbibition Processes

The only initial condition considered in this study is  $\hat{S}(z,0) = 0$ . This condition implies that the unscaled initial saturation is  $S_i$  (see equation (11)). Throughout this paper it is assumed that  $S_i$  is a small value at which  $k_{rw}$  is effectively zero.

Boundary Condition I - The classical boundary conditions studied by Philip in one-phase flow analysis are:

$$\left. \begin{aligned} \hat{S}(0, \hat{t}) &= 1.0 \\ \hat{S}(\infty, \hat{t}) &= 0 \end{aligned} \right\} \quad (49)$$

These conditions require some explanation. Equation (39), used in the derivation of equation (44), has meaning only when the capillary pressure is a single-valued function of saturation. For some porous materials, there exists a range of capillary pressures near zero throughout which  $\hat{S} = 1.0$ . The capillary pressure at the upper limit of this range is the pressure at which the non-wetting phase becomes discontinuous in the imbibition process. The scaled value of this capillary pressure is designated by the symbol  $\hat{P}_d$ . For capillary pressures less than  $\hat{P}_d$ , equation (39) does not apply. Therefore, throughout this work, the boundary condition  $\hat{S}(0, \hat{t}) = 1.0$  implies that the capillary pressure at  $\hat{z} = 0$  is  $\hat{P}_d$  unless stated otherwise.

Boundary Conditions II - A second boundary condition of interest is the case of ponded water on the surface of the porous medium. This condition can occur in the field during intense rainfall or during flood irrigation. Explicitly, boundary conditions II are:

$$\left. \begin{aligned} \hat{S}(0, \hat{t}) &= 1.0 \\ \hat{P}_w(0, \hat{t}) &= \text{constant} \\ \hat{S}(\infty, \hat{t}) &= 0 \end{aligned} \right\} \quad (50)$$

Boundary Conditions III - The boundary condition of constant flux at  $\hat{z} = 0$  is considered:

$$\left. \begin{aligned} \hat{q}_w(0, \hat{t}) &= \text{constant} \\ \hat{S}(L, \hat{t}) &= 0 \\ \hat{q}_a(L, \hat{t}) &= 0 \end{aligned} \right\} \quad (51)$$

These boundary conditions imply that the saturation at  $z = 0$  is a function of time. In the field, this boundary condition can occur during constant rainfall of low intensity.

Boundary Conditions IV - The final set of boundary conditions studied is for a finite medium. In this case, the conditions specified are constant liquid pressure at  $\hat{z} = 0$  and no flux across the plane at  $\hat{z} = L$ .

$$\left. \begin{aligned} \hat{P}_w(0, \hat{t}) &= \text{constant} \\ \hat{q}_w(L, \hat{t}) &= \hat{q}_a(L, \hat{t}) = 0 \end{aligned} \right\} \quad (52)$$

Solution for the Horizontal Case

The objective of the following analysis of horizontal imbibition is to gain further insight into the physics of two-phase flow in porous media. In particular, the intent is to investigate the influence that the displaced non-wetting phase exerts upon imbibition of liquids into porous media. The results of this section serve as a starting point for the analysis of vertical infiltration.

Almost all theoretical investigations of the imbibition process existing at this time have used the Richards' equation as the starting point. The Richards' equation is derived upon the assumption that the resistance to the movement of the non-wetting phase is negligible in comparison to the resistance to flow of the wetting phase. This assumption is, in turn, based on the condition that the viscosity of the non-wetting phase is small compared to the viscosity of the wetting phase. However, situations exist in which the channels through which the non-wetting phase must move within the porous material become so small that the resistance to flow is significant in spite of the small viscosity value for the non-wetting phase.

For horizontal imbibition equation (44) reduces to:

$$\frac{\partial}{\partial x} \left( D \frac{\partial \hat{S}}{\partial x} \right) - \hat{V} f'_w \frac{\partial \hat{S}}{\partial x} = \frac{\partial \hat{S}}{\partial t} \quad (53)$$

in which the vertical coordinate  $\hat{z}$  has been replaced by the horizontal coordinate  $\hat{x}$ .

There are two unknown dependent variables ( $\hat{S}$  and  $\hat{V}$ ) in equation (53), and it is necessary to introduce a second independent equation in involving these two variables. Combining equations (37), (39), and (43) for the case of horizontal flow yields:

$$\hat{q}_w = \hat{V} f'_w - D \frac{\partial \hat{S}}{\partial x} \quad (54)$$

Equation (54) is used to relate the total velocity  $\hat{V}$  to the imbibition rate  $\hat{q}_o$ . Evaluation of equation (54) at  $\hat{x} = 0$  (at  $\hat{S} = 1.0$ ) shows that:

$$\hat{q}_o(\hat{t}) = \hat{V}(\hat{t}) \quad (55)$$

where  $\hat{q}_o$  is the imbibition rate. This is true because  $f'_w(1) = 1$  and  $D(1) = 0$ . The cumulative volume of imbibed fluid at any time is calculated by integrating the saturation profile. Since the imbibition rate is the time derivative of the cumulative volume, then the total velocity can be expressed by:

$$\hat{V}(\hat{t}) = \frac{d}{dt} \int_0^{1.0} \hat{x} d\hat{S} \quad (56)$$

Equations (53) and (56) are to be solved simultaneously.

The Boltzman transformation of variables is introduced:

$$\psi = \hat{x} \hat{t}^{-1/2} \quad (57)$$

It is well known that the initial and boundary conditions

$$\left. \begin{aligned} \hat{S}(0, \hat{t}) &= 1.0 \\ \hat{S}(\infty, \hat{t}) &= 0 \\ \hat{S}(\hat{x}, 0) &= 0 \end{aligned} \right\} \quad (58)$$

are invariant under the transformation (57). It is assumed that the solution  $\hat{S}(\hat{x}, \hat{t})$  to the simultaneous equations (53) and (56) is transformed by equation (57) to the form  $\hat{S} = \hat{S}(\psi)$  or equivalently  $\psi = \psi(\hat{S})$ . The assumption is valid if the simultaneous equations reduce to an equation with  $\hat{S}$  and  $\psi$  the only variables.

Solving equation (57) for  $x$  and substituting into equation (56) results in:

$$\hat{V}(\hat{t}) = \frac{\hat{t}^{-1/2}}{2} \int_0^{1.0} \psi \, d\hat{S} \quad (59)$$

The integral in equation (59) is denoted by the constant  $\bar{\psi}$ . That is:

$$\bar{\psi} = \int_0^{1.0} \psi \, d\hat{S} \quad (60)$$

Substituting equation (59) into equation (53) results in:

$$\frac{\partial}{\partial x} \left( D \frac{\partial \hat{S}}{\partial x} \right) - \frac{\bar{\psi}}{2} \hat{t}^{-1/2} f'_w \frac{\partial \hat{S}}{\partial x} = \frac{\partial \hat{S}}{\partial \hat{t}} \quad (61)$$

Making the transformation (57) in equation (61) yields:

$$\hat{t}^{-1} \frac{\partial}{\partial \psi} \left( D \frac{\partial \hat{S}}{\partial \psi} \right) - \frac{\bar{\psi} \hat{t}^{-1}}{2} f'_w \frac{\partial \hat{S}}{\partial \psi} = \hat{t}^{-1} \psi \frac{\partial \hat{S}}{\partial \psi} \quad (62)$$

Explicit reference to  $\hat{t}$  is eliminated from equation (62) by cancellation, and since  $\hat{S}$  and  $\psi$  are the only variables remaining, equation (62) becomes an ordinary differential equation:

$$\frac{d}{d\psi} \left( D \frac{d\hat{S}}{d\psi} \right) = \frac{1}{2} (\bar{\psi} f'_w - \psi) \frac{d\hat{S}}{d\psi} \quad (63)$$

To summarize, the solution of equation (53) subject to conditions (58) is expressed by:

$$\hat{x} = \psi(\hat{S}) \hat{t}^{1/2} \quad (64)$$

where  $\psi(\hat{S})$  satisfies

$$\frac{d}{d\psi} \left( D \frac{d\hat{S}}{d\psi} \right) = \frac{1}{2} (\bar{\psi} f'_w - \psi) \frac{d\hat{S}}{d\psi} \quad (65)$$

subject to:

$$\left. \begin{aligned} \hat{S} &= 1; \psi = 0 \\ \hat{S} &= 0; \psi \rightarrow \infty \end{aligned} \right\} \quad (66)$$

#### Solution for Horizontal Case in Terms of Fractional Flow Function

It was pointed out in the discussion of  $f_w$  that, when capillary gradients and gravitational forces are neglected,  $f_w$  can be interpreted as the ratio of  $q_w$  to  $V$ . An analogous expression can be defined for cases in which capillary (or saturation) gradients are retained:

$$F_{w1} = \frac{\hat{q}_w}{V} = f_w - \frac{D}{V} \frac{\partial \hat{S}}{\partial x} \quad (67)$$

Equation (67) follows immediately from equation (54).

It is of interest to derive the solution to the horizontal flow problem in terms of  $F_{w1}$ , because an integral equation for  $F_{w1}$  which is relatively easy to evaluate can be derived from equation (65). Furthermore, the approximate solution for vertical infiltration presented in the next section is most easily derived from  $F_{w1}$ .

Making the variable transformation defined by equation (57) in equation (67) results in:

$$F_{w1}(\hat{S}) = f_w(\hat{S}) - \frac{2D(\hat{S})}{\bar{\psi}} \frac{d\hat{S}}{d\psi} \quad (68)$$

It is noted from equation (68) that  $F_{w1}$  is a function of  $\hat{S}$  only. Therefore, the equation of continuity (equation (27)), when written in terms of  $F_{w1}$ , becomes:

$$\hat{V} \frac{dF_{w1}}{d\hat{S}} \frac{\partial \hat{S}}{\partial x} = - \frac{\partial \hat{S}}{\partial \hat{t}} \quad (69)$$

The solution to equation (69) is of the form  $\hat{S} = \hat{S}(\hat{x}, \hat{t})$ . Calculation of the total differential of  $\hat{S}$  gives:

$$d\hat{S} = \frac{\partial \hat{S}}{\partial x} dx + \frac{\partial \hat{S}}{\partial \hat{t}} d\hat{t} \quad (70)$$

Equation (70), when applied to a constant value of saturation  $\hat{S}_j$  reduces to the differential equation:

$$\frac{\partial \hat{S}}{\partial x} \Big|_{\hat{S}_j} dx_j + \frac{\partial \hat{S}}{\partial \hat{t}} \Big|_{\hat{S}_j} d\hat{t} = 0 \quad (71)$$

where  $\hat{x}_j$  is the coordinate of the plane whose saturation is  $\hat{S}_j$ .

Solving equation (69) and (71) simultaneously yields:

$$\hat{V} \frac{d F_{w1}}{d \hat{S}} = \frac{d \hat{x}}{d \hat{t}} \quad (72)$$

in which the j-subscript notation has been abandoned since the meaning of equation (72) is clear. Using equation (59) for  $\hat{V}$  and integrating equation (72) subject to  $\hat{x} = 0$  at  $\hat{t} = 0$ , yields:

$$\hat{x} = \frac{d F_{w1}}{\psi} \frac{d \hat{S}}{d \hat{t}} \hat{t}^{1/2} \quad (73)$$

Equation (73) is the desired equation for the saturation profile. The solution represented by equation (73) is similar to that obtained by Buckley and Leverett (5) who derived an expression of the same form in 1942. These investigators, however, neglected capillarity as a driving force.

Equation (73) is only a formal solution so long as  $F_{w1}$  remains unknown. Equation (69) can be written as:

$$\frac{d F_{w1}}{\psi d \hat{S}} = \psi \frac{d \hat{S}}{d \hat{S}} \quad (74)$$

Integration of equation (74) results in the expression relating  $F_{w1}$  and  $\psi$ :

$$F_{w1}(\hat{S}) = \frac{1}{\psi} \int_0^{\hat{S}} \psi d \hat{S}' \quad (75)$$

From the foregoing, it is clear that the solution represented by equation (64) and that by equation (73) are consistent formulations. In the case of the solution represented by equation (64), a differential equation for  $\psi(\hat{S})$  is known. The differential equation for  $\psi(\hat{S})$  is easily converted to a differential equation for  $F_{w1}$  by using equation (75). The result is:

$$\frac{d^2 F_{w1}}{d \hat{S}^2} = \frac{2 D(\hat{S})}{\psi^2 (f_w - F_{w1})} \quad (76)$$

An integral equation for  $F_{w1}$  is obtained by integrating equation (76). The result is:

$$F_{w1}(\hat{S}) = \frac{2}{\psi^2} \int_0^{\hat{S}} \int_{S'}^{1.0} \frac{D}{(F_{w1} - f_w)} d S'' d S' \quad (77)$$

A procedure for the solution of equation (77) has been worked out. The method consists of selecting a first approximation to  $F_{w1}$  and improving upon the initial estimate by iteration. The first estimate of  $F_{w1}$  should satisfy the properties which are deduced as follows:

Equation (75) implies that  $F_{w1}(1) = 1$  and that  $F_{w1}(0) = 0$ . Thus, equation (75) establishes the end points of  $F_{w1}(\hat{S})$ . The boundary condition that  $\hat{x} = 0$  at  $\hat{S} = 1.0$  requires that  $d F_{w1}/d \hat{S}$  be zero at  $\hat{S} = 1.0$ . In view of equation (73), one can argue on physical grounds that  $d F_{w1}/d \hat{S}$  is a monotonically decreasing function of  $\hat{S}$ . Otherwise, equation (73) predicts that two distinct values of saturation exist at the same plane in the porous medium; a physical absurdity. One final property of  $F_{w1}$  should be noted. The value of  $F_{w1}$  must be greater than  $f_w$  at all points on the open interval  $0 < \hat{S} < 1.0$ .

The properties of  $F_{w1}$  listed above allow one to make a rational first approximation to  $F_{w1}$ , which is then used to compute the integrals on the right side of equation (77). Since  $F_{w1}(1) = 1$ , the value of  $\psi$  can be computed. The next step is to calculate a new estimate of  $F_{w1}$  which is accomplished from equation (77). Using the second estimate of  $F_{w1}$ , the process is repeated. Iteration is continued until the most recent estimate of  $F_{w1}$  is only negligibly different from the previous estimate. Numerical examples of this procedure have been carried out and the method has been found to converge very rapidly.

#### Solution for the Vertical Case - Boundary Conditions I

The solution under boundary conditions I is derived first, and then extended for boundary conditions II.

The procedure used to derive an approximate solution to the infiltration problem is called the "method of undetermined functions" by Ames (2). The differential equation of interest can be represented by:

$$L U = 0 \quad (78)$$

where  $L$  is a non-linear, partial-differential operator in general. The solution  $U$  of equation (78) is a function of the space coordinates and time,  $U = U(\bar{r}, t)$ , where  $\bar{r}$  is the position vector in the domain  $R$ . When  $U(\bar{r}, t)$  is an exact solution then:

$$\int_R L U(\bar{r}, t) d \bar{r} = 0 \quad (79)$$

holds. When the exact solution is approximated by  $\underline{U}$ , the integrand in equation (79) is not identically zero but is equal to a residual which is a function of  $\bar{r}$  and  $t$ . Let  $\underline{U}$  be of the form

$$\underline{U} = \underline{U} [g(\bar{r}, h(t))] \quad (80)$$

where  $\underline{U}$  and  $g$  are known functions and  $h(t)$  is to be determined so that the residual is small in some sense. The expression

$$\int_R L U [g(\bar{r}, h(t))] d \bar{r} = 0 \quad (81)$$

is interpreted as meaning the average residual over the domain  $R$  is zero. Furthermore, equation (81) is a differential equation for the underdetermined function  $h(t)$ .

There are several variations and generalizations of the technique outlined above, but the rather special case presented is sufficient to introduce the development in the following pages.

For the case of vertical flow, it is more convenient to work with equation (44) after it has been transformed so that  $\hat{z}$  is the dependent variable. The formulas

$$\frac{\partial \hat{S}}{\partial z} = \frac{1}{\partial z / \partial \hat{S}} \quad (82)$$

and

$$\frac{\partial \hat{S}}{\partial t} = - \frac{\partial z / \partial \hat{t}}{\partial z / \partial \hat{S}}, \quad (83)$$

when applied to equation (44), accomplish the desired transformation. The result is:

$$\frac{\partial}{\partial \hat{S}} \left( \frac{D}{\partial z / \partial \hat{S}} \right) - \hat{V} \frac{df_w}{d\hat{S}} - \frac{dE}{d\hat{S}} = - \frac{\partial \hat{z}}{\partial \hat{t}} \quad (84)$$

In equation (84), the variable  $\hat{z}$  is analogous to the solution  $U$  in the discussion of the method of undetermined functions, and  $\hat{S}$  plays the same role as  $\bar{r}$ .

Integrating equation (84) over  $\hat{S}$  yields:

$$\left[ \frac{D}{\partial z / \partial \hat{S}} \right]_0^{1.0} - V f_w \left[ \right]_0^{1.0} - E \left[ \right]_0^{1.0} = - \int_0^{1.0} \frac{\partial \hat{z}}{\partial \hat{t}} d\hat{S} \quad (85)$$

Since both  $D(\hat{S})$  and  $E(\hat{S})$  are zero at the end points of the saturation scale and  $f_w(0) = 0$  and  $f_w(1) = 1$ , equation (85) reduces to:

$$\hat{V}(\hat{t}) - \int_0^{1.0} \frac{\partial \hat{z}}{\partial \hat{t}} d\hat{S} = 0 \quad (86)$$

Equation (86) is comparable to equation (79) in this case.

The approximation to the exact solution is constructed from the general fractional-flow function for vertical flow; that is

$$F_{wz}(\hat{S}, \hat{t}) = f_w - \frac{D(\hat{S})}{V(\hat{t})} \frac{\partial \hat{S}}{\partial z} + \frac{E(\hat{S})}{V(\hat{t})} \quad (87)$$

Comparison of equation (87) with equation (67) shows that:

$$F_{wz} = F_{w1} + \frac{E(\hat{S})}{V(\hat{t})}, \quad (88)$$

where  $F_{w1}$  is the general fractional-flow function for horizontal flow. At small times, when  $\hat{V}(\hat{t})$  is large,  $F_{wz} \approx F_{w1}$ . Also, for values of  $\hat{S}$  near 1.0,  $E(\hat{S}) \approx 0$ . Therefore, near  $\hat{S} = 1.0$ , the vertical fractional-flow function is approximated by the horizontal function at all times. For these reasons,  $F_{wz}$  is considered as a perturbation of  $F_{w1}$  for the purpose of constructing an approximation to the saturation profile. Based on this approximation, equation (87) becomes:

$$F_{w1} = f_w - \frac{D}{V} \frac{\partial \hat{S}}{\partial z} + \frac{E}{V} \quad (89)$$

Solving equation (89) for  $\partial \hat{S} / \partial z$ , applying equation (82), and integrating yields the following approximate solution:

$$\hat{z} = - \int_{\hat{S}}^{1.0} \frac{D d\hat{S}'}{(f_w - F_{w1}) \hat{V} + E} \quad (90)$$

Equation (90) corresponds to the approximation given by equation (80). The function  $\hat{V}(\hat{t})$  in equation (90) is the equivalent of  $h(t)$  in equation (80).

Substitution of equation (90) into equation (86) results in:

$$\hat{V} = - \int_0^{1.0} \left\{ \frac{\partial}{\partial \hat{t}} \int_{\hat{S}}^{1.0} \frac{D d\hat{S}'}{(f_w - F_{w1}) \hat{V} + E} \right\} d\hat{S} \quad (91)$$

Interchanging the order of differentiation and integration and integrating over  $\hat{S}$  by parts yields:

$$\hat{V} = - \frac{d}{dt} \int_0^{1.0} \frac{\hat{S} D d\hat{S}}{(f_w - F_{w1}) \hat{V} + E} \quad (92)$$

Carrying out the indicated differentiation and rearranging gives:

$$\int_0^{1.0} \frac{\hat{S} D (F_{w1} - f_w)}{E^2 \hat{V}} \frac{d\hat{V}/d\hat{t}}{\left( \frac{F_{w1} - f_w}{E} \hat{V} - 1 \right)^2} d\hat{S} = -1 \quad (93)$$

which is a differential equation for  $\hat{V}(\hat{t})$ . The solution of equation (93) subject to  $1/\hat{V} = 0$  at  $\hat{t} = 0$  is:

$$\begin{pmatrix} 1.0 \\ 0 \end{pmatrix} \frac{\hat{S} D(F_{w1} - f_w)}{E^2} \left\{ \frac{1}{\frac{F_{w1} - f_w}{E} \hat{V} - 1} \right. \\ \left. + \ln \left( 1 - \frac{E}{(F_{w1} - f_w) \hat{V}} \right) \right\} d\hat{S} = \hat{t} \quad (94)$$

The function  $\hat{V}(\hat{t})$  obtained from equation (94) is an approximation to the infiltration rate, and the saturation distribution is approximated by equation (90).

#### Solution for the Vertical Case - Boundary Conditions II

During vertical imbibition under boundary conditions II, it is assumed that a zone in which  $\hat{S} = 1.0$  moves into the medium. The coordinate of the plane between the region in which  $\hat{S} = 1.0$  and the region where  $\hat{S} < 1.0$  will be denoted by  $\hat{z}_f$ . Equation (53) applies for  $\hat{z} \geq \hat{z}_f$ , and Darcy's equation in the form

$$\hat{q}_0(\hat{t}) = \frac{\mu_a}{\mu_w} k_{rw}(1) \left( \frac{\hat{P}_o + \hat{P}_d - \hat{P}_{af}}{\hat{z}_f} + 1 \right) \quad (95)$$

applies for  $\hat{z} \leq \hat{z}_f$ . In equation (95),  $\hat{P}_o$  is the scaled wetting-phase pressure at  $\hat{z} = 0$ ,  $\hat{P}_d$  is the capillary pressure at  $\hat{z} = \hat{z}_f$ ,  $\hat{P}_{af}$  is the non-wetting phase pressure at  $\hat{z}_f$ ,  $k_{rw}(1)$  is the relative permeability to the wetting phase at  $\hat{S} = 1.0$ , and  $\hat{q}_0(\hat{t})$  is the infiltration rate.

It is convenient to use a linear transformation of variable defined by

$$\xi = \hat{z} - \hat{z}_f(\hat{t}) \quad (96)$$

The following formulas hold for any function of  $\hat{z}$  and  $\hat{t}$ :

$$\frac{\partial}{\partial \hat{z}} \Big|_{\hat{t}} = \frac{\partial \xi}{\partial \hat{z}} \Big|_{\hat{t}} \frac{\partial}{\partial \xi} = \frac{\partial}{\partial \xi} \Big|_{\hat{t}} \quad (97)$$

and

$$\frac{\partial}{\partial \hat{t}} \Big|_{\hat{z}} = \frac{\partial}{\partial \hat{t}} \Big|_{\xi} - \frac{d\hat{z}_f}{dt} \frac{\partial}{\partial \xi} \Big|_{\hat{t}} \quad (98)$$

Applying these formulas to equation (44) results in:

$$\frac{\partial}{\partial \xi} \left( D \frac{\partial \hat{S}}{\partial \xi} \right) - \hat{V} \frac{\partial f_w}{\partial \xi} - \frac{\partial E}{\partial \xi} + \frac{dz_f}{dt} \frac{\partial \hat{S}}{\partial \xi} = \frac{\partial \hat{S}}{\partial \hat{t}} \quad (99)$$

The associated boundary conditions are:

$$\left. \begin{aligned} \hat{S} &= 1.0 & \text{at } \xi &= 0 \\ \hat{S} &= 0 & \text{at } \xi &= \infty \end{aligned} \right\} \quad (100)$$

Equation (99) can be expressed with  $\xi$  as the dependent variable by making use of equations (82) and (83). The result is:

$$\frac{\partial}{\partial \hat{S}} \left( \frac{D}{\partial \xi / \partial \hat{S}} \right) - \frac{dE}{d\hat{S}} - \hat{V} \frac{df_w}{d\hat{S}} + \frac{dz_f}{dt} = - \frac{\partial \xi}{\partial \hat{t}} \quad (101)$$

Integration of equation (101) over  $\hat{S}$  yields:

$$\hat{V} - \frac{dz_f}{dt} = \int_0^{1.0} \frac{\partial \xi}{\partial \hat{t}} d\hat{S} \quad (102)$$

As in the previous case, the infiltration rate is equal to the total velocity  $\hat{V}$ . Therefore, the variables  $\hat{V}$  and  $\hat{z}_f$  are related through equation (95) which, after rearrangement and differentiation becomes:

$$\frac{dz_f}{dt} = - \frac{\mu_w}{\mu_a k_{rw}(1)} \frac{(\hat{P}_o + \hat{P}_d - \hat{P}_{af})}{\left( \frac{\mu_w}{\mu_a k_{rw}(1)} \hat{V} - 1 \right)^2} d\hat{V}/d\hat{t} \quad (103)$$

The differentiation in equation (103) was carried out assuming that the quantity  $(\hat{P}_o + \hat{P}_d - \hat{P}_{af})$  is a constant. This condition and its relation to experiment is discussed in detail in a later section.

Let

$$A = \frac{\mu_w}{\mu_a k_{rw}(1)} (\hat{P}_o + \hat{P}_d - \hat{P}_{af}) \quad (104)$$

Using equation (104) in (103) and substituting into equation (102) yields:

$$\hat{V} + \frac{A}{\left( \frac{\mu_w}{\mu_a k_{rw}(1)} \hat{V} - 1 \right)^2} \frac{d\hat{V}}{dt} = \int_0^{1.0} \frac{\partial \xi}{\partial \hat{t}} d\hat{S} \quad (105)$$

In the region in which the saturation  $\hat{S}$  is less than unity the approximation

$$\xi = - \int_{\hat{S}}^{1.0} \frac{D(\hat{S}) d\hat{S}'}{(f_w - F_{w1}) \hat{V} + E} \quad (106)$$

applies.

Substitution of equation (106) into equation (105), integrating by parts over  $\hat{S}$ , and differentiating with respect to time yields:

$$\left\{ \frac{A}{\hat{V} \left\{ \frac{\mu_w}{\mu_a k_{rw}(1)} \hat{V} - 1 \right\}^2} + \int_0^{1.0} \frac{\hat{S} D d\hat{S}}{\hat{V} \left\{ \left( \frac{f_w - f_{w1}}{\hat{V} + E} \right)^2 \right\}} \right\} \frac{d\hat{V}}{dt} = -1 \quad (107)$$

which is a differential equation for  $\hat{V}$ .

The solution of equation (107) subject to  $1/\hat{V} = 0$  at  $t = 0$  is:

$$A \left\{ \frac{1}{\frac{\mu_w}{\mu_a k_{rw}(1)} \hat{V} - 1} + \ln \left( 1 - \frac{\mu_a}{\mu_w k_{rw}(1)} \hat{V} \right) \right\} + \int_0^{1.0} \frac{\hat{S} D (F_{w1} - f_w)}{E^2} \left\{ \frac{1}{\frac{F_{w1} - f_w}{\hat{V} - 1}} + \ln \left( 1 - \frac{E}{F_{w1} - f_w} \hat{V} \right) \right\} d\hat{S} = \hat{t} \quad (108)$$

### Solution for the Vertical Case - Boundary Conditions III

The conditions specified in this case are constant liquid flux at  $z = 0$ . The situation to be studied is one of counter-current flow. This means that the flux vectors  $\hat{q}_a$  and  $\hat{q}_w$  are equal in magnitude and of opposite sense. Therefore, the total velocity  $V(t)$  is zero. Conditions of counter-current flow can be caused by an impermeable boundary at some distance below the infiltrating surface. The displaced air escapes by flowing upward through the wetted zone.

Equation (44) reduces to:

$$\frac{\partial}{\partial z} \left( D \frac{\partial \hat{S}}{\partial z} \right) - E \frac{\partial \hat{S}}{\partial z} = \frac{\partial \hat{S}}{\partial t} \quad (109)$$

for counter-current infiltration. The liquid flux is given by a modified form of equation (37):

$$\hat{q}_w = -D(\hat{S}) \frac{\partial \hat{S}}{\partial z} + E(\hat{S}) \quad (110)$$

Since the infiltration rate is constant, equation (110) evaluated at  $\hat{z} = 0$  is:

$$\hat{q}_0 = -D(\hat{S}_0) \frac{\partial \hat{S}}{\partial z} \Big|_{z=0} + E(\hat{S}_0) \quad (111)$$

where  $\hat{S}_0$  is the saturation at  $\hat{z} = 0$ . The resistance to flow tends to become larger as the wetted zone grows. In order that  $\hat{q}_0$  remain constant,

this tendency must be compensated by an increasing conductivity to the liquid in the wetted zone. Therefore,  $\hat{S}_0$  is an increasing function of time. The primary interest in the solution to this problem is to ascertain  $\hat{S}_0 = \hat{S}_0(\hat{t})$ .

The approach used to obtain an approximate solution for this case again involves a fractional flow function. Neither of the fractional flow functions already considered can be used here since  $\hat{V}(\hat{t}) = 0$ . Instead the following function is defined:

$$F_{w3} \equiv \hat{q}_w / \hat{q}_0 = \frac{-D}{q_0} \frac{\partial \hat{S}}{\partial z} + \frac{E}{q_0} \quad (112)$$

Introducing equation (112) into equation (109) results in:

$$\hat{q}_0 \frac{\partial}{\partial z} F_{w3}(\hat{z}, \hat{t}) = - \frac{\partial \hat{S}}{\partial t} \quad (113)$$

Applying equations similar to equations (82) and (83) to equation (113), an equation with  $\hat{S}$  and  $\hat{t}$  as the independent variables is obtained:

$$\hat{q}_0 \frac{\partial}{\partial \hat{S}} F_{w3}(\hat{S}, \hat{t}) = \frac{\partial \hat{z}}{\partial \hat{t}} \quad (114)$$

Differentiating equation (114) with respect to  $\hat{S}$  yields:

$$\hat{q}_0 \frac{\partial^2 F_{w3}}{\partial \hat{S}^2} = \frac{\partial^2 \hat{z}}{\partial \hat{S} \partial \hat{t}} \quad (115)$$

The derivatives on the right of equation (115) have a physical interpretation which lends itself to experimental investigation. The derivative  $\partial \hat{z} / \partial \hat{t}$  can be regarded as the velocity of a particular saturation. The second derivative indicates how the velocity of particular saturations compare at any time. Experimental evidence (figure 29) indicates that the velocity of a particular saturation is approximately constant during constant infiltration. Even more important is the observation that particular saturations (capillary pressures) propagate at approximately the same velocity. This means that the right-hand side of equation (115) is approximately zero. Therefore:

$$\frac{\partial^2 F_{w3}}{\partial \hat{S}^2} = 0 \quad (116)$$

The conclusion that all saturations in the range characterized by large capillary gradients should propagate with the same velocity (not necessarily constant) has been justified on analytic grounds by Lefur (see discussion in reference 15). For the case of constant infiltration, it appears that this approximation is valid even for saturations near the maximum saturation that can be obtained.

Integration of equation (116) yields:

$$F_{w3} = \alpha(\hat{t})\hat{S} + \beta(\hat{t}) \quad (117)$$

where  $\alpha$  and  $\beta$  are constants (with respect to  $\hat{S}$ ) of integration. The conditions that  $F_{w3}(0, \hat{t}) = 0$  and that  $F_{w3}(\hat{S}_0, \hat{t}) = 1$  reduce equation (117) to:

$$F_{w3}(\hat{S}, \hat{t}) = \frac{\hat{S}}{\hat{S}_0(t)} \quad (118)$$

Substitution of equation (118) into equation (112) and rearrangement results in:

$$\frac{\partial \hat{z}}{\partial \hat{S}} = \frac{D(\hat{S})}{E(\hat{S}) - q_0 \hat{S} / \hat{S}_0(t)} \quad (119)$$

Integration of equation (119) yields the equation for the saturation profile:

$$\hat{z}(\hat{S}, \hat{t}) = \int_{\hat{S}}^{\hat{S}_0} \frac{D}{\frac{q_0 \hat{S}}{\hat{S}_0} - E} d\hat{S}' \quad (120)$$

The unknown  $\hat{S}_0(\hat{t})$  in equation (120) is determined by requiring that continuity be satisfied. That is:

$$\hat{q}_0 \hat{t} = \int_0^{\hat{S}_0} \hat{z} d\hat{S} \quad (121)$$

Substitution of equation (120) into equation (121) yields:

$$\hat{q}_0 \hat{t} = \int_0^{\hat{S}_0} \int_{\hat{S}}^{\hat{S}_0} \frac{D}{\frac{q_0 \hat{S}}{\hat{S}_0} - E} d\hat{S}' d\hat{S} \quad (122)$$

Integrating equation (122) by parts gives:

$$\hat{q}_0 \hat{t} = \int_0^{\hat{S}_0(\hat{t})} \frac{\hat{S} D}{\frac{q_0 \hat{S}}{\hat{S}_0} - E} d\hat{S} \quad (123)$$

Equation (123) is the desired equation for  $\hat{S}_0(\hat{t})$ . Computations are made by selecting a value of  $\hat{S}_0$ , computing the integrand and carrying out the indicated integration. The time corresponding to the particular value of  $\hat{S}_0$  selected is computed by dividing equation (123) by  $\hat{q}_0$ .

During the early stages of constant infiltration, the term  $\partial \hat{S} / \partial \hat{z} |_{\hat{z}=0}$  in equation (111) becomes less negative with increasing time and ultimately approaches zero. In this case  $\hat{q}_0 = E(\hat{S}_0)$ , and the saturation at  $\hat{z} = 0$  becomes constant. When this condition occurs, the liquid conductivity has adjusted to the minimum value which will permit infiltration to proceed at the rate  $\hat{q}_0$  due to the driving force of gravity.

The resistance to the escape of air is accounted for because it has been incorporated into  $E(\hat{S})$ . Therefore, the larger the applied infiltration rate, the larger  $E(\hat{S})$  must be for infiltration to persist at the same rate after capillary driving forces become negligibly small. Since  $E(\hat{S})$  exhibits a maximum, say at  $\hat{S}_m$ , it is concluded that any infiltration rate  $\hat{q}_0$  greater than  $E(\hat{S}_m)$  cannot continue indefinitely. This is because any increased conductivity to liquid gained by a further increase in  $\hat{S}_0$  is offset by a decreased conductivity to the escaping air. Since the system can no longer transmit liquid at the rate  $\hat{q}_0$  when  $\hat{S}_0 = \hat{S}_m$ , ponding of the liquid on the surface occurs. The boundary conditions change at this time. No attempt is made in this work to analyze the problem after ponding occurs.

#### Solution for Vertical Case - Boundary Conditions IV

The final set of boundary conditions studied is the case in which liquid is provided at the surface at a constant positive pressure, and the air can escape through the upper surface of the medium only. In this case counter-current flow of the air phase does not begin immediately as in the case of constant liquid flux at the upper surface. This is because the air is trapped by the wetting front and compresses until the capillary pressure at the upper surface reaches a threshold value at which air begins to escape from the top of the column.

Again it is assumed that a region in which  $\hat{S} = 1.0$  develops in the medium. In the treatment of boundary conditions II, equation (108) was derived on the basis that the factor  $A$  defined in equation (104) is constant. Under the conditions of interest in this section,  $A$  is not constant because  $\hat{P}_{af}$  increases as the air phase is compressed. Equation (108) can be used, however, by assuming that over a time period  $\Delta t$ , infiltration proceeds as if  $\hat{P}_{af}$  were constant during that time period.

The computational procedure is as follows. A family of cumulative infiltration curves is prepared using equation (108) for various values of  $\hat{P}_{af}$  starting with  $\hat{P}_{af} = 0$  and increasing until  $A = 0$ . Each curve represents the cumulative infiltration as a function of time assuming that  $\hat{P}_{af}$  (i.e.  $A$ ) is constant. An example family of curves are shown in Figure 3.

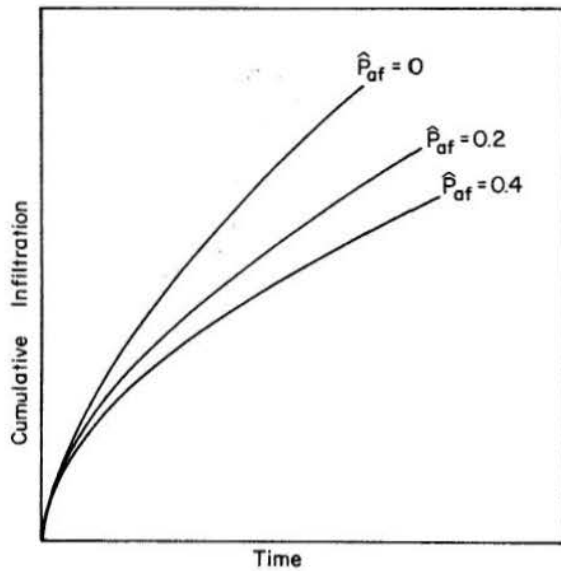


FIGURE 3 - Example curves showing the relationship between cumulative infiltration and time for various values of  $\hat{p}_{af}$ .

Neglecting gradients in the air phase, the ideal gas law is used to compute the cumulative infiltration corresponding to each value of  $\hat{p}_{af}$  used in constructing the above family of curves. The relationship is:

$$\hat{Q} = v_i - \frac{\bar{P} v_i}{(\hat{p}_{af} + \bar{P})}, \quad (124)$$

where  $v_i$  is the dimensionless air volume at the initial condition and  $\bar{P}$  is the dimensionless atmospheric pressure.

It is assumed that each increment of infiltration takes place as if  $\hat{p}_{af}$  remains constant at the value of  $\hat{p}_{af}$  obtained at the beginning of the increment. The time at which a given cumulative infiltration exists is obtained from the family of curves which have been constructed.

The above procedure can be used only until the air pressure has built up to a value equal to  $\hat{p}_o + \hat{p}_d$ . Therefore, the developments contained in this section are inadequate to predict the entire process. Furthermore, for many porous materials, the value of  $\hat{p}_d$  may be zero or not well defined. In such cases the above method is of little use.

## EXPERIMENTAL PROCEDURES

The infiltration phenomenon was studied experimentally by subjecting two different porous materials to infiltration tests. One of the materials used is a river sediment called Poudre sand. Poudre sand is an unconsolidated sand with a relatively wide distribution of pore sizes and a permeability that is of the same order of magnitude as many soils.

A consolidated sand known as Berea sandstone was selected as the second material. This material is relatively permeable when compared to other naturally occurring consolidated materials and is very homogeneous in the direction parallel to the bedding planes.

The wetting fluid used throughout this study was a light hydrocarbon oil called Phillips core test fluid\*. This fluid is referred to simply as "oil" in the following sections.

### Measurement of Hydraulic Properties

The functions  $P_c(S)$  and  $k_{rw}(S)$ , for unconsolidated materials, are often measured by using two different samples of the porous medium. On one sample the capillary pressure-saturation function is measured, and on the other, the relationship between  $P_c$  and  $k_{rw}$  is determined. By combining these two relationships, the functional relationship between  $k_{rw}$  and  $S$  is deduced. This method has the distinct disadvantage of requiring two samples which, in practice, are very difficult to prepare so that they are very nearly identical.

In this work, the functions  $P_c(S)$  and  $k_{rw}(S)$  for the Poudre sand were measured simultaneously on the same sample by utilizing gamma-ray attenuation equipment to determine the saturation. The technique used in this study to measure the capillary pressure and relative permeability has been described by various investigators (3,8,29). In this case, however, the soil column was placed in a framework which supported the gamma-ray attenuation equipment. Measurements of  $P_c$ ,  $k_{rw}$  and  $S$  were taken at a series of steady states as described in the above references.

The source of gamma radiation used was a 100 millicurie Americium isotope. The radiation was directed through the test section of the soil column by means of a collimator. The collimator consisted of a lead column approximately six inches long constructed with a 1/16" x 3/4" slot through the center of the column. The long dimension of the slot was oriented parallel to the axis of the soil column. This was done so that the measurements obtained were representative of the bulk density of approximately 1/3 of the test section in the soil column. A collimator with a cylindrical cross-section of the same area would have resulted in measurements representative of the material in only a very small portion of the test section.

Gamma radiation passing through the soil column was detected by a photomultiplier tube and read out on a portable scaler in units of counts per unit of time.

The gamma-ray equipment was constructed so that the source and detector could be shifted laterally. In this way, a standard could be measured each time a reading on the soil column was taken. Adjustable stops were constructed to insure that the source and detector were returned to exactly the same position each time. A schematic diagram of the experimental set-up is shown in Figure 4.

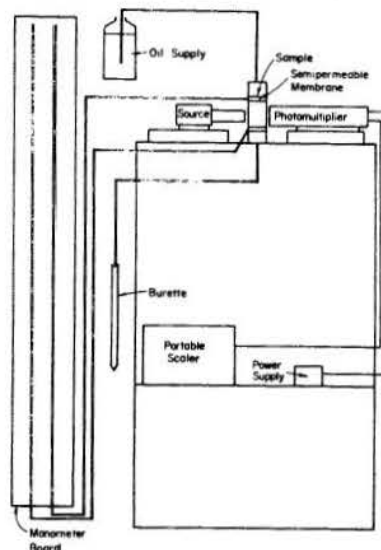


FIGURE 4 - Schematic diagram of Gamma-ray attenuation equipment.

Calibration of the equipment was made by taking a reading on the soil column when the soil was air dry and again after the soil had been vacuum saturated. This procedure established the end points of the calibration curve. It was observed in preliminary tests that the number of counts per unit of time varied linearly with the degree of saturation for a particular soil. Therefore it was assumed that the calibration curve was a straight line joining the end points. The readings were plotted as percent of the standard reading in each case. After the completion of the experiment the test section was removed and the saturation determined gravimetrically as a check on the linearity of the calibration curve.

No attempt was made to measure the relative permeability to air as a function of saturation for the Poudre sand.

The hydraulic properties of the Berea sandstone were measured using techniques that differ only slightly from techniques described in previous investigations. In the case of consolidated materials, combining the  $P_c(S)$  and  $k_{rw}(P_c)$  curves to obtain the  $k_{rw}(S)$  relationship can be done with confidence because the same sample can be used for both experiments. Therefore, the gamma radiation equipment was not employed to measure saturation. The relationship between  $k_{rw}$  and  $P_c$  was measured using techniques similar to those discussed in references 8 and 29.

\* Manufactured by Phillips Petroleum Company, Special Products Division, Bartlesville, Oklahoma.

A technique for measuring  $P_c$  as a function of  $S$  on consolidated materials has been described by White (34). White's technique was modified during the early stages of the desaturation portion of the experiment. The leveling bottles which were used by White to determine the capillary pressure were replaced by a pressure transducer which sensed the pressure in the core continuously. The capillary pressure was increased by evaporating the liquid from the core with a fan. At a particular value of capillary pressure, the corresponding saturation was determined by removing the sandstone plug from the capillary barriers and weighing it. Corey (3) in an unpublished study of this technique has concluded that the method gives reliable results as long as the conductivity of the core does not become too low. The principal advantage of the method is that it is much faster than other methods.

During the imbibition portion of the experiment, evaporation from the sample was minimized by placing the apparatus in an aluminum box. The bottom of the box was covered with approximately 1/8" of oil in an attempt to keep the air surrounding the core saturated with the liquid vapor. The top of the box was covered with a saran wrap which was easily removed when the core was to be weighed.

The technique reported by White for determining when the core should be weighed at any particular capillary pressure does not apply when the experiment is one of imbibition. The interface in the observation tube continually moves after a step reduction in the capillary pressure. The rate of movement of the interface is large immediately following the change in capillary pressure, but decreases to a small value which is representative of the evaporation rate from the sample. It was difficult to ascertain exactly when the imbibition rate was equal to the evaporation rate. Therefore, it was assumed that the imbibition and evaporation rates were equal when the movement of the interface in the observation tube was apparently constant. The saturation of the core was determined at this time. To check this assumption, the core was replaced after a particular measurement and a second measurement was taken approximately two hours later. The two weight determinations were found to agree. It is believed, however, that this technique can lead to significant errors unless the evaporation rate is kept quite small.

Determination of the relative permeability to air as a function of saturation was accomplished by techniques developed by Corey (7). On the imbibition cycle, the saturation in the core sample was increased by applying the oil on the lateral surface of the core with a damp cloth. It was found that highly erratic measurements of air permeability resulted if any oil was applied to the ends of the core. After the liquid application, the core was allowed to remain in a weighing bottle until the oil was uniformly distributed throughout the core. During the early stages of the experiment when the core was nearly dry, measurements were made when the oil distribution in the core appeared uniform to the eye. When the saturation had been increased to a value at which visual detection of a uniform oil distribution was no longer possible, measurements were made after an arbitrary length of time. Several of these measurements were checked by repeating the reading at some later time before the next increment of liquid was applied.

### Infiltration Subject to Boundary Conditions III

Infiltration tests were made on columns subjected to boundary conditions II, III and IV. The experimental procedures used for studying infiltration under conditions II and IV were quite similar and will be discussed together. The procedures employed in the study of infiltration subject to conditions III are sufficiently different to warrant a separate discussion.

Of major interest in the study of constant-rate infiltration is the development of the capillary pressure or saturation profile and the time at which ponding occurs on the surface. All of the constant-rate experiments were performed under conditions of counter-current flow of air. Under such conditions, the capillary pressure cannot be determined by measuring the liquid pressure only, because it cannot be assumed that the air pressure is atmospheric at all times. Therefore, the experiments were designed to measure both the air and liquid pressure at various positions in the column as functions of time. A schematic diagram of the experimental design is shown in Figure 5.

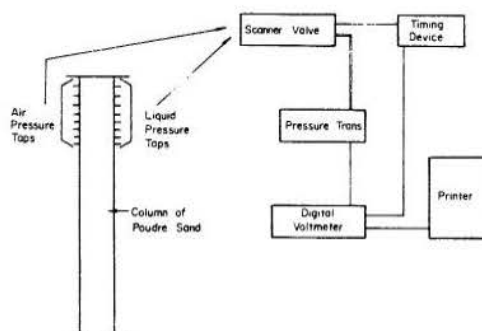


FIGURE 5 - Schematic diagram of equipment setup for constant rate experiments.

The column in which the Poudre sand was placed was constructed of short lucite sections sealed by rubber O-rings between each section. The one-centimeter sections in the upper portions of the column were designed so that both liquid and air pressure could be measured at the center of each section. In one-half of each section was a tensiometer which sensed the liquid pressure. The air pressure was measured through an opening covered with a fine wire screen on the opposite half of each section. A total of seven such sections made up the upper portion of the soil column. The bottom of the column was sealed which forced the air to escape in a counter-current direction.

The pressure in both the liquid and the air were measured by means of a pressure transducer and a scanner valve. Leads from the liquid and air taps for each measuring section were connected to adjacent ports in the scanner valve. The center port of the scanner

was connected to the pressure transducer. By rotating the scanner valve, the pressure at each tap was measured. The scanner valve was rotated at equal intervals of time by means of a timing device which automatically opened and closed an electrical circuit at equal intervals of time. In addition to the pressure at taps in the column, two calibration pressures were measured each time the scanner valve made a revolution.

The pressure transducer converted the pressure to a voltage output which was digitized by a digital volt meter and printed on paper tape. A large number of data points were generated during each experiment. Therefore, a digital computer was used to reduce the data.

At the beginning of each experiment run, the tensiometers were vacuum saturated and then subjected to a suction of approximately 100 cm of oil. This was accomplished by "hanging" a 100 cm column of oil in a Tygon tube from each tensiometer. The tubing was then clamped which caused the tensiometers to remain at the desired suction. Each section was then placed in its proper position in the columns. The next step was placing the Poudre sand in the column. This was done by adding the sand through a funnel with a long rigid stem which reached to the bottom of the column. The column was made extra long so that when the desired bulk density was obtained the extra length of column could be removed. This procedure helped to insure that the properties of the soil immediately at the surface were as near like those of the rest of the column as possible. Even so, some disturbance of the soil at the top of the column always occurred.

During the packing procedure the tensiometers were in contact with the dry soil. However, because the liquid pressure in the tensiometer was maintained at a negative pressure head of about 100 cm of oil, imbibition into the soil was very slight.

The timing device was started simultaneously with the introduction of liquid at a predetermined constant rate at the top of the column. In some cases, the rate of air outflow was measured during the experiment by means of a soap-film flow meter.

#### Infiltration Subject to Boundary Conditions II and IV

Columns of both Poudre sand and Berea sandstone were subjected to infiltration tests during this portion of the study. The column on which the Poudre sand tests were made was a continuous lucite tube. An end plate was cemented to the bottom of the column which kept the sand in place.

The sand was placed in the column with the funnel already described and packed to the desired bulk density. The degree of homogeneity of the packing was determined by measuring the air-pressure head at a number of points along the column while flowing air at a constant rate through the column. Typical results are shown in Figure 6.

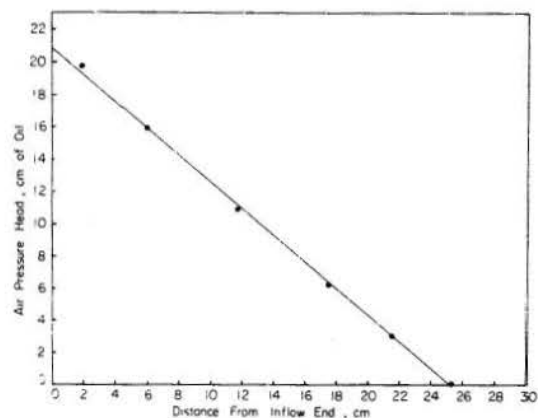


FIGURE 6 - Typical curve showing the degree of homogeneity obtained in the Poudre sand columns.

A perfectly homogeneous packing would have resulted in all the pressure-head measurements lying on a straight line. This ideal situation could not be realized, however. Therefore, the columns were considered to be satisfactorily homogeneous if the head-loss distribution was comparable to that shown in Figure 6. It was found that, when the columns were packed to the proper bulk density and the degree of homogeneity was satisfactory, the maximum deviation in air permeability was 4.3 percent of the average of 11 samples. On 6 samples, the permeability to oil at the maximum saturation on the imbibition cycle was determined. It was found that the ratio of air permeability to this value of oil permeability was very nearly constant. The maximum deviation of this ratio from the average was 1.9 percent of the average.

After it was determined that a particular column was properly packed, two column sections were attached to the top of the column which were used in the application of the oil during the test. The first was a section, 1 cm in height, which was sealed to the top of the column by an O-ring. A thin rubber membrane was stretched over the top of this section and held in place with a second section by clamping the two together. A predetermined quantity of oil was placed in the upper column section, and was retained by the membrane. A constant head burette was attached to the upper section which maintained the oil at the desired level. To begin the experiment, the membrane was pierced with a sharp object which allowed the oil to infiltrate the soil. Piercing the tightly stretched membrane caused it to practically disintegrate. The cumulative volume taken up by the soil was recorded as a function of time.

The semi-infinite case was simulated using the column described above which was 25.4 cm long by allowing the displaced air to escape freely from the bottom of the column. The validity of simulating a

semi-infinite medium in this manner is discussed in the following section of this work.

Infiltration tests into finite media were conducted using similar experimental procedures. Finite media of different lengths were simulated by using the 25.4 cm column to which was attached an air tank. The volume of air in the tank was varied to represent different lengths of column. The pressure in the air was monitored through a pressure tap by means of a pressure transducer and a brush recorder. In these experiments, no attempt was made to measure the capillary pressure distribution. Figure 7 is a schematic diagram of the experimental apparatus for the infiltration experiments.

Experiments on the Berea sandstone differed only slightly from those on the Poudre sand column. The sandstone column was a core, 2 inches in diameter, which was cut parallel to natural bedding planes. The lateral surface was sealed with an epoxy paint manufactured by the Carboline Company. Holes were drilled in the coating at intervals along the column to which pressure taps were cemented. Lucite sections of a design similar to those used for the Poudre sand were attached to the ends of the column.

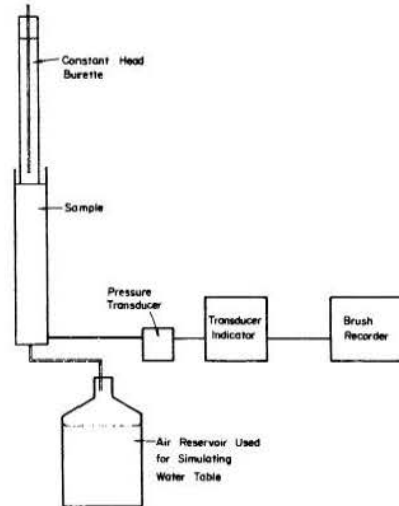


FIGURE 7 - Schematic diagram of equipment setup for infiltration experiments.

RESULTS AND DISCUSSION

It was pointed out in the first section of this paper that most of the theoretical work done on the imbibition of liquids into porous media has been carried out assuming that the resistance to flow of the air phase is negligible. It is appropriate, therefore, to discuss the significant results of the two-phase flow analysis with respect to the conclusions of a one-phase flow analysis wherever possible. Experimental results are discussed concurrently.

Imbibition in Semi-infinite Media

The imbibition of liquid into porous materials is many times referred to as a "diffusion" phenomenon. This terminology arises because the Richards' equation, when expressed in terms of saturation, is the same form as the classic diffusion equation. The diffusion coefficient or "diffusivity" is highly dependent on the degree of saturation.

When the problem of horizontal imbibition is analyzed from the standpoint of two-phase flow, it is found that the shape of the saturation profile and therefore the rate of imbibition is a function of the behavior of the integrand of equation (77), particularly for values of  $\hat{S}$  near 1.0.

It is noted that the integrand in equation (77) is indeterminate at  $\hat{S} = 1.0$ . The author has not been successful to date in attempts to evaluate this function in the limit as  $\hat{S}$  approaches 1.0 except for the case when  $k'_{ra}(1.0) \neq 0$ . However, numerical calculations indicate that the integrand is not a monotonically increasing function of  $\hat{S}$ , but instead reaches a maximum value near  $\hat{S} = 0.98$  and then decreases to some limiting value as  $\hat{S}$  approaches 1.0.

A maximum of the integrand in equation (77) at, say,  $\hat{S} = \hat{S}_j$  means that there exists an inflection point in the saturation profile at  $\hat{S}_j$ . The saturation profile for  $\hat{S} > \hat{S}_j$  is essentially the Buckley-Leverett profile which is obtained by neglecting capillary gradients. This is in agreement with the work of Brustkern and Morel-Seytoux (4).

The saturation profile predicted from the solution of the Richards' equation has no inflection point near  $\hat{S} = 1.0$ . It should be pointed out that it would be very difficult to detect the inflection in the profile experimentally with the present methods of measuring saturation under dynamic conditions. Figure 8 is an example of the saturation profile calculated from equation (73) in which  $F_{w1}$  was computed from equation (77). The  $F_{w1}$  curve is shown in Figure 9.

It is noted that the inflection is so subtle that it cannot be observed on a graph of this scale. The point is not entirely academic, however, because it has a bearing on the limiting value approached by the infiltration rate during vertical imbibition.

Equation (94) is the approximate solution derived for infiltration into a semi-infinite medium subject to the boundary condition that  $\hat{S} = 1.0$  at  $\hat{z} = 0$ .

The limiting value of the infiltration rate  $\hat{V}$  as  $\hat{t}$  becomes large is given by:

$$\lim_{\hat{t} \rightarrow \infty} \hat{V} = \lim_{\hat{S} = 1.0} \frac{E}{F_{w1} - f_w} \quad (125)$$

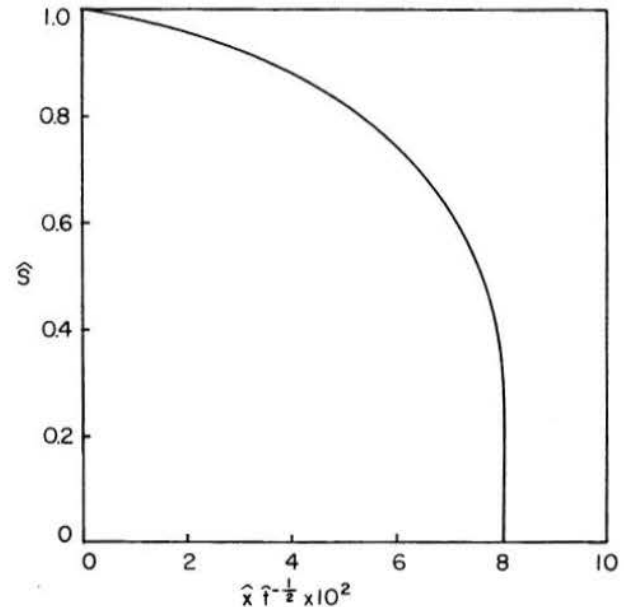


FIGURE 8 - Example saturation profile for horizontal imbibition.

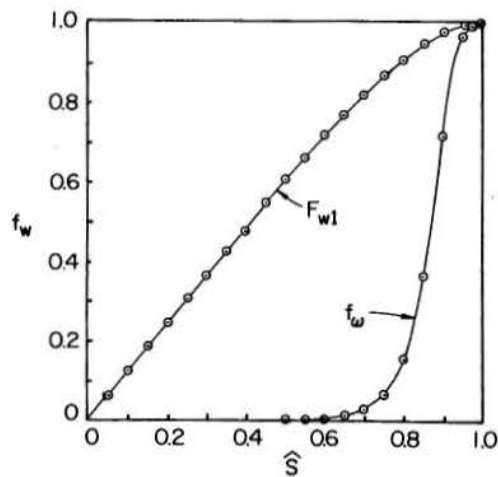


FIGURE 9 -  $F_{w1}$  and  $f_w$  curves used for calculation of the profile in Figure 8.

For the case when  $k'_{ra}(1.0) \neq 0$ , the above limit is equal to  $\mu_a k_{rw}(1)/\mu_w$  which is the scaled value of the hydraulic conductivity at  $\hat{S} = 1.0$  and the limiting value of the infiltration rate predicted from the Richards' equation. Numerical calculations indicate that for the case in which  $k'_{ra}(1.0) = 0$  the limit in equation (125) is a value somewhat smaller than  $\mu_a k_{rw}(1)/\mu_w$ , although this cannot be concluded with certainty. Brustkern and Morel-Seytoux (4) found the limiting value of the infiltration rate to be less than that predicted from the Richards' equation.

Morel-Seytoux (15) has shown that, in the limit as time becomes very large, the actual fractional flow  $F_{w2}$  must approach a curve defined by  $f_w + E(S)/V$  as modified by the Welge tangent construction. The reader is referred to this reference for a lucid discussion of this result. The approximation used in the present work does not satisfy this requirement except near  $\hat{S} = 1.0$ . Therefore, the saturation profile at large times predicted in the present analysis is not correct throughout the entire range of saturations. The major result of the incorrect saturation profile at large times is to overestimate the influence of gravitational forces on the infiltration phenomenon. This results in predicted infiltration rates which are too high when the gravitational forces become significant relative to the capillary driving forces. The magnitude of the error in predicted infiltration rates has not been definitely established.

In the derivation of equation (108) for infiltration subject to a ponded-liquid boundary condition, it is assumed that a zone in which  $\hat{S} = 1.0$  develops in the porous medium. This was done as a convenient approximation. From a rigorous theoretical standpoint such a zone does not occur. This is concluded from the fact that  $D(\hat{S})$  is zero at  $\hat{S} = 1.0$ . From the definition of  $E(\hat{S})$  and  $D(\hat{S})$  (equations (36) and (43)) it is evident that  $D(\hat{S})$  approaches zero at  $\hat{S} = 1.0$  as a result of  $k_{ra}$  approaching zero at that saturation. This in turn implies that the resistance to flow of the air becomes infinite as  $\hat{S}$  approaches 1.0. Therefore, it is concluded that all of the continuous air phase is never displaced from the material. In fact, this conclusion is related to the fact that the saturation profile exhibits an inflection near  $\hat{S} = 1.0$ .

The result of this approximation is that equation (108) is not entirely consistent. This is evident because the first term in brackets predicts the limiting value of the infiltration rate to be  $\mu_a k_{rw}(1)/k_{ra}$  and the second term in brackets predicts the limiting value to be that given in equation (125). Because the difference between these two limiting values is small, the effect on numerical calculations is insignificant except at very large times. A comparison between calculated and measured infiltration for the Poudre sand is shown in Figure 10.

The calculations for the Poudre sand were made from the data shown in Figures 11 and 12. It is observed in Figure 12 that  $S_o$  for the Poudre sand is 0.91. The initial condition was the air-dry sand for which  $S_i = 0$ . Using these values the measured

data were replotted in terms of  $\hat{S}$ . The result is shown in Figures 13 and 14. The relative permeability to air for the Poudre sand shown in Figure 13 is not measured data. This curve was calculated from formulas given by Brooks and Corey. The capillary pressure curve in Figure 14 was idealized slightly by making the straight-line extrapolation from  $\hat{S} = 0.9$  to  $\hat{S} = 1.0$  as shown. This resulted in a value of

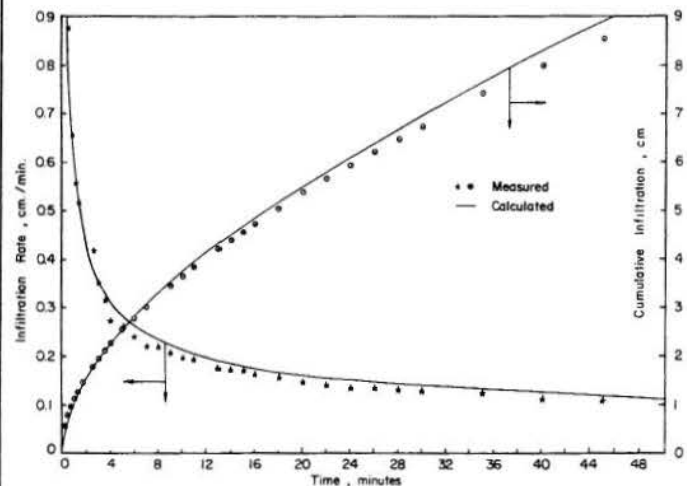


FIGURE 10 - Comparison of theory and experiment for infiltration in Poudre sand.

$P_d/\rho g$  of 22 cm of oil. Experimental data presented in the next section provides a justification for this modification of the measured data.

It was pointed out in the derivation of equation (108) that the factor  $A$  defined by equation (104) was assumed constant. This implies that  $P_{af}$  is constant. For infiltration into semi-infinite media, the assumption further implies that  $P_{af}$  is zero.

Experimental measurements of the pressure in the air phase in Poudre sand near the upper surface of the medium were made in order to check this assumption. These results are shown in Figure 15. In these experiments the air was allowed to escape freely from the bottom of the column. It is noted that the length of column has a marked effect on the air pressure buildup. This is due, of course, to the increased resistance to flow in the longer column. In view of these results, air taps along the column of Poudre sand were left open to the atmosphere so that the air could more readily escape and the infiltration experiments were repeated. The infiltration data from these experiments on the 25.4 cm columns of Poudre sand agreed with that from columns in which the air could escape only from the bottom to the same degree that a given data set could be reproduced. It was not possible to detect a difference in the infiltration data that could be directly attributed to air pressure buildup.

It should be emphasized that the above conclusions are based on observations taken from a column of Poudre sand 25.4 cm long. It is expected that these conclusions cannot be extrapolated to columns which are much longer because a significant air pressure buildup persisted in the 51 cm column for up to 3 minutes.

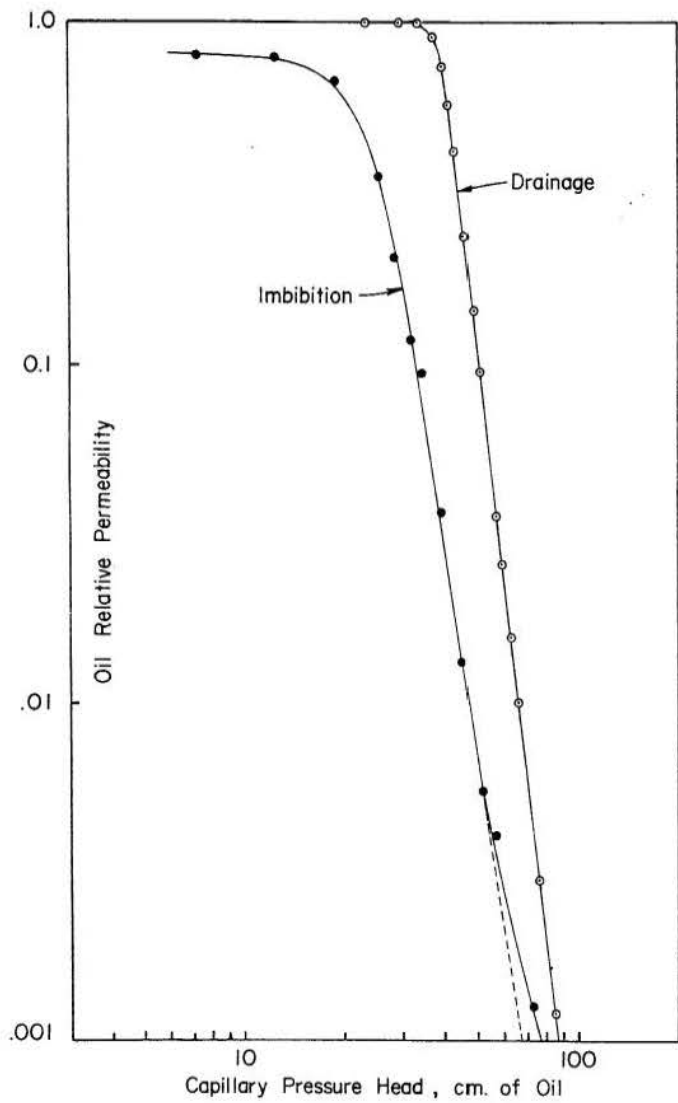


FIGURE 11 - Relative permeability as a function of capillary pressure head for Poudre sand.

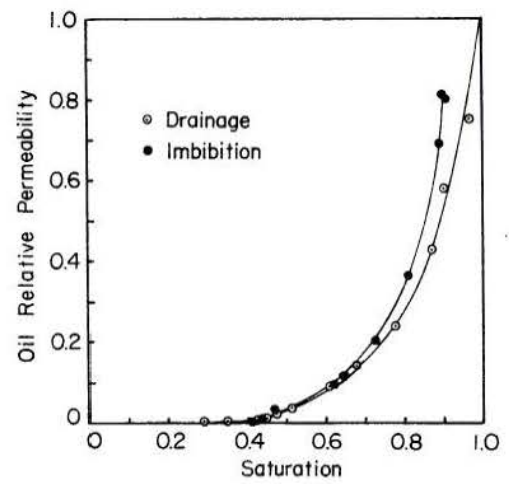
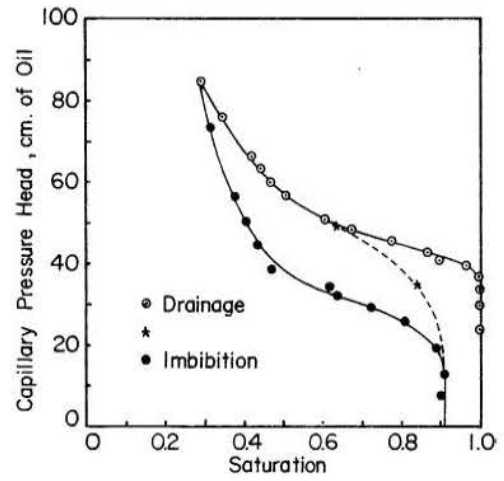


FIGURE 12 - Capillary pressure head and relative permeability as functions of saturation for Poudre sand.

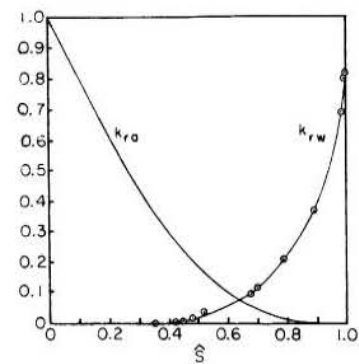


FIGURE 13 - Relative permeability as a function of  $\hat{S}$  for Poudre sand.

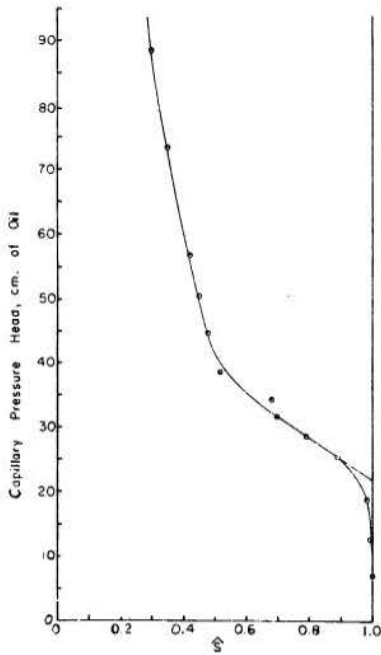


FIGURE 14 - Capillary pressure head as a function of  $S$  for Poudre sand.

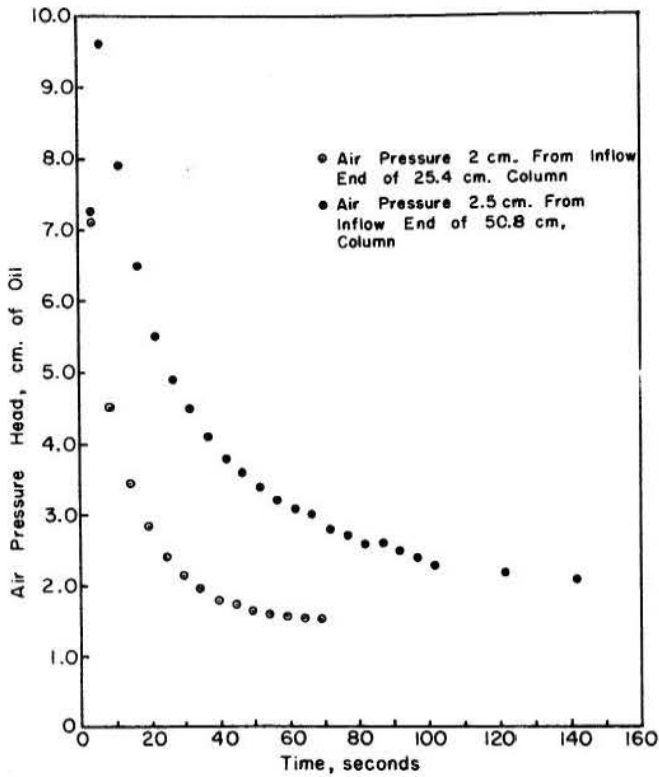


FIGURE 15 - Air pressure head in columns of Poudre sand.

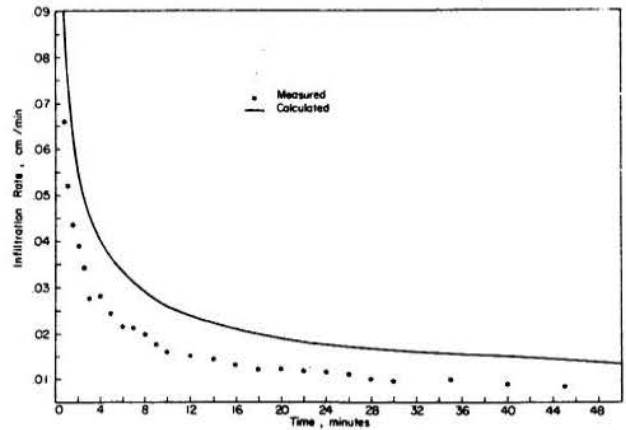


FIGURE 16 - Comparison of theory and experiment for infiltration in Berea sandstone.

Figure 16 is a comparison of experimental data with calculations from equation (94) for the Berea sandstone. There is considerable discrepancy between the calculated and measured values in this case. The calculated curve is displaced from the measured one by an approximately constant factor. This indicates that the calculated curve has the correct shape. Therefore the fact that the influence of gravity is over-estimated in equation (94) does not appear to explain the discrepancy. The calculation is very sensitive to the slope of the capillary pressure curve near  $S = 1.0$ , and small errors in this curve could produce the observed difference. The data from which these calculations were made are shown in Figures 17 and 18.

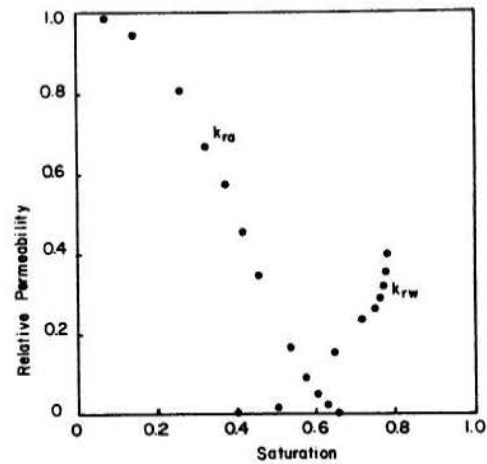


FIGURE 17 - Relative permeability as a function of saturation for Berea sandstone.

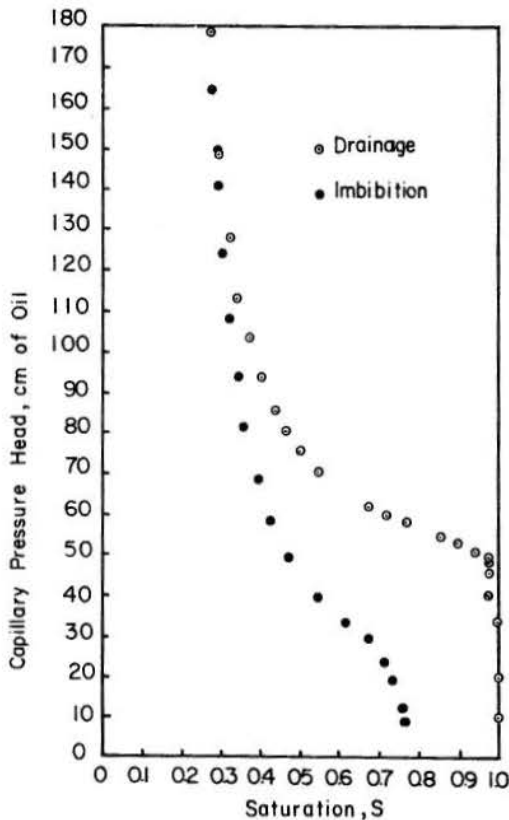


FIGURE 18 - Capillary pressure head as a function of saturation for Berea sandstone.

#### Infiltration in Finite Media

The procedures discussed in the section entitled Boundary Conditions IV were employed to compute the solid curves shown in Figure 19 for Poudre sand. The value of  $P_d/\rho g$  used in these calculations is 22.0 cm. The points shown in this graph are measured cumulative infiltration data for various effective column lengths. Apparently the calculation procedure for finite media is adequate to predict the cumulative infiltration as a function of time until the air pressure head has increased to  $P_d/\rho g + P_o/\rho g$  (equal to 23.6 cm in this case). The calculation procedure cannot be carried beyond this point.

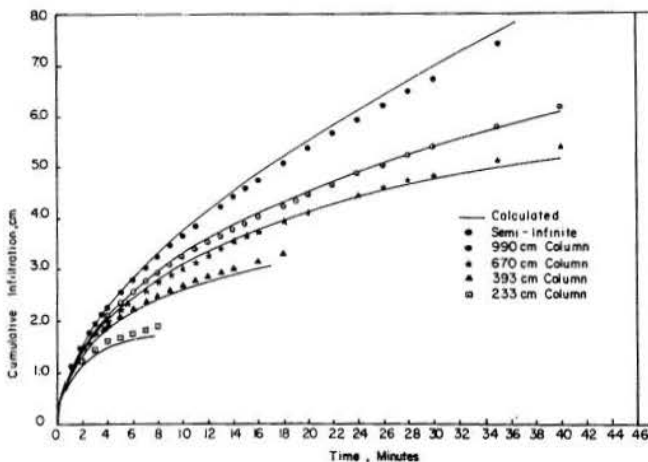


FIGURE 19 - Comparison of theory and experiment for infiltration in finite columns of Poudre sand.

The data from infiltration tests into finite media are shown in Figures 20 through 24. The infiltration rates plotted on all graphs were calculated from the cumulative infiltration curves by the formula:

$$(q)_t = \frac{(Q_{t+\Delta t} - Q_t)/\Delta t + (Q_t - Q_{t-\Delta t})/\Delta t}{2} \quad (126)$$

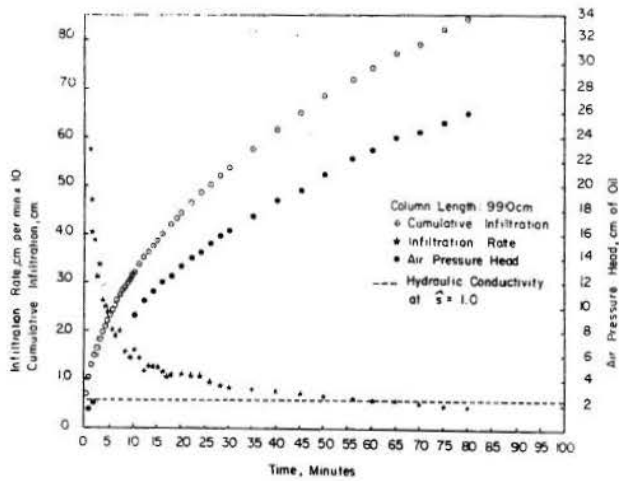
where  $(q)_t$  is the infiltration rate at time  $t$ .

This procedure provides some smoothing of the calculated infiltration rates. This was necessary because the volume of oil in the constant head burette used to measure the cumulative infiltration changed in discrete increments rather than continuously. At any particular time, the volume of oil in the burette could be determined to within  $\pm 0.1 \text{ cm}^3$ , but the volume of oil in the porous medium could differ from the determined value by an additional  $\pm 0.2 \text{ cm}^3$ , which was the volume of discrete changes in the burette.

It is observed that in each of the Figures 20-24 that the infiltration rate decreased to a value lower than the hydraulic conductivity at  $\hat{S} = 1.0$ . It is interesting to note, however, that the pressure head in the air phase (when the infiltration rate was equal to the hydraulic conductivity at  $\hat{S} = 1.0$ ) was approximately 24 cm of oil in each case. The range was from 26 cm to 22 cm for the 5 different cases. Based on the assumption that a zone in which  $\hat{S} = 1.0$  develops in the medium, one would expect the infiltration rate to be equal to the hydraulic conductivity when the air pressure head is equal to 23.6 cm (see equation (95)). This observation provides some justification for the assumption that such a zone develops. It should be remembered, however, that this assumption was made as a convenient approximation to the actual situation.

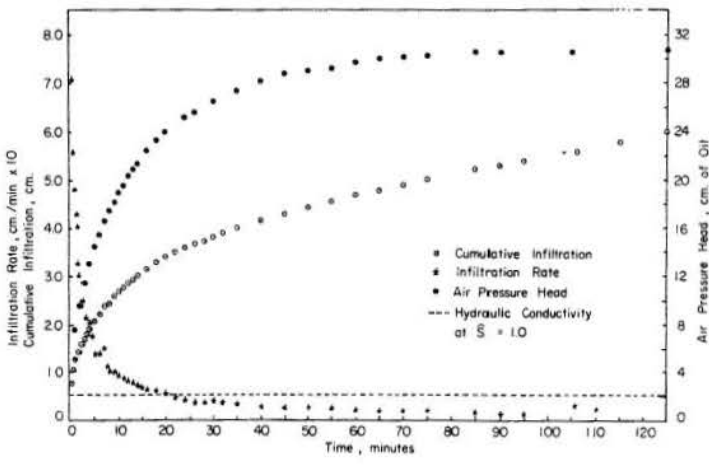
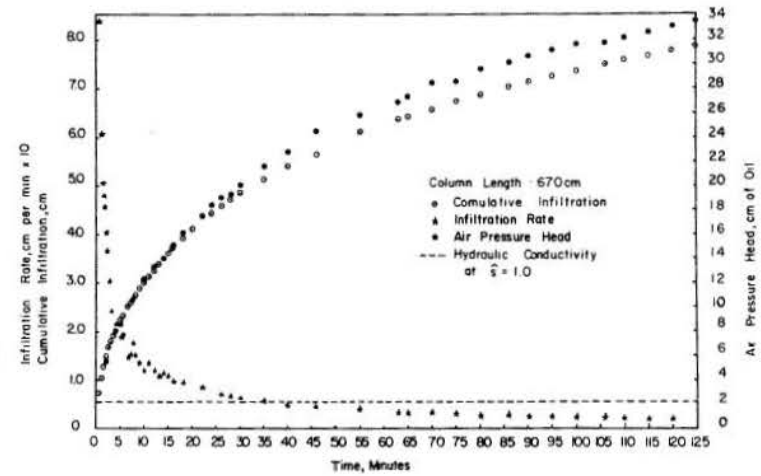
The Figures 23 and 24, it is seen that a sharp decrease in the air pressure head and a corresponding increase in the infiltration rate occurred after the air pressure head reached a value of about 33 cm of oil. Escape of the air from the top of the column was observed a few seconds before the beginning of the pressure decrease. In the case of 990, 670 and the 393-cm columns, the wetting front reached the bottom of the column before the air pressure buildup was sufficient to allow the air to escape. In addition, there are indications of an air leak in the 393-cm column.

The fact that the air pressure head builds up to values significantly higher than 23.6 cm before air begins to escape is evidence that the saturation in a portion of the column near the surface decreases. Initially, the air pressure is zero in the column and near the top of the column the saturation  $\hat{S}$  is very near 1.0. Before the air can escape, the saturation must decrease to provide air permeability. The increase in capillary pressure associated with the decrease in saturation takes place along the dotted curve shown in Figure 12 rather than the primary imbibition loop. Therefore, the increase in capillary pressure near the surface necessary to provide the air permeability required for air escape is considerably greater than would be predicted from the primary imbibition loop. Since the liquid pressure at the surface is constant, the increase in capillary pressure must be provided by an increase in air pressure. The infiltration rate decreases to values less than the hydraulic conductivity at  $\hat{S} = 1.0$  because the air pressure buildup represents a retarding force and



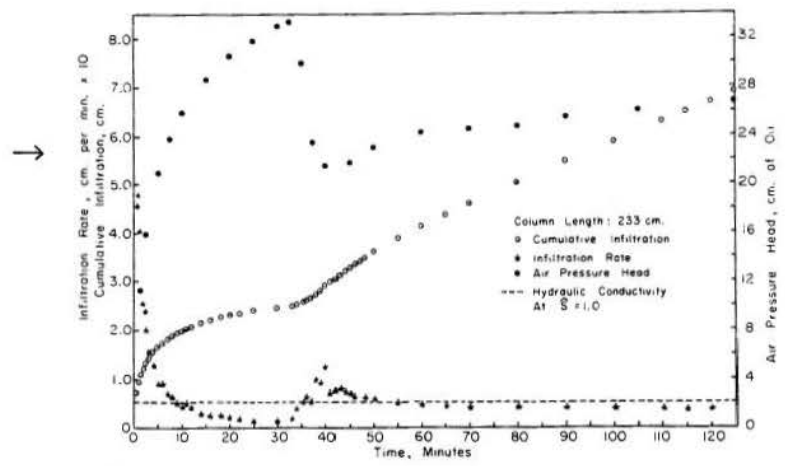
← FIGURE 20 - Infiltration in a column of Poudre sand - 990 cm equivalent length.

FIGURE 21 - Infiltration in a column of Poudre sand - 670 cm equivalent length. →



← FIGURE 22 - Infiltration in a column of Poudre sand - 393 cm equivalent length.

FIGURE 23 - Infiltration in a column of Poudre sand - 233 cm equivalent length. →



causes a reduced permeability to liquid by increasing the capillary pressure.

The infiltration rates in Figures 23 and 24 show that after counterflow of air begins, a sharp increase in infiltration rate occurs. The rate increases to a peak and then declines to a value below the hydraulic conductivity corresponding to  $\hat{S} = 1.0$ . The limiting value of the infiltration rate is lower in the finite columns than in those open at the bottom because of the resistance to the counterflowing air.

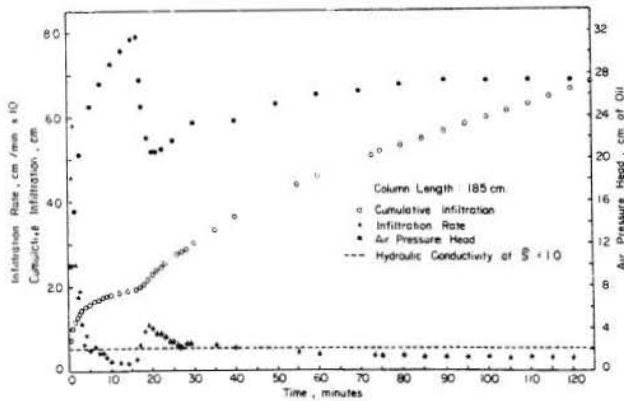


FIGURE 24 - Infiltration in a column of Poudre sand - 185 cm equivalent length.

Simultaneously with the observation of the counterflow of air a slight disturbance of the surface of the Poudre sand was noticed. The air escaped near this contact area in small bubbles through small holes which were formed in the sand. It is believed that the formation of the worm-like holes by the escaping air is the reason for the sharp pressure decrease observed shortly after counterflow began. This could account for the increase in infiltration rates to values higher than hydraulic conductivity at  $\hat{S} = 1.0$ .

To test this theory, a Berea sandstone column was subjected to the same test. The results are shown in Figure 25.

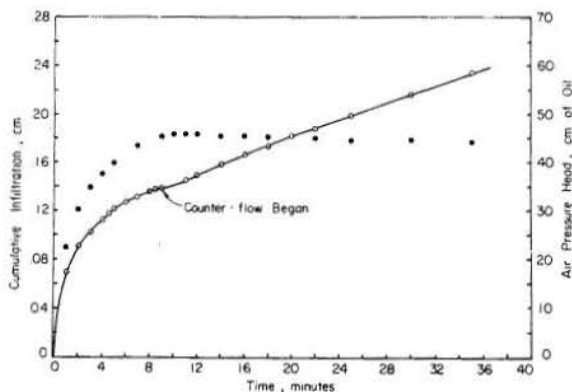


FIGURE 25 - Infiltration in a column of Berea sandstone - 17.4 cm equivalent length.

The decrease in pressure associated with the beginning of counterflow observed for the Poudre sand did not occur in the Berea. The slight decline in pressure near the termination of the experiment is believed to be due to the development of an air leak.

The counterflowing air was observed to be concentrated at two points on the surface of the sandstone. Although the Berea is very homogeneous parallel to its natural bedding planes, the presence of the bedding planes makes it quite anisotropic. This fact could explain the escape of the air being concentrated in two places.

#### Constant Rate Infiltration

Columns of Poudre sand were subjected to constant rate infiltration tests with the objective of observing the development of the capillary pressure profile and the factors affecting the time at which ponding on the surface occurs.

The capillary pressure head as a function of time at seven positions in the column of Poudre sand are shown in Figure 26.

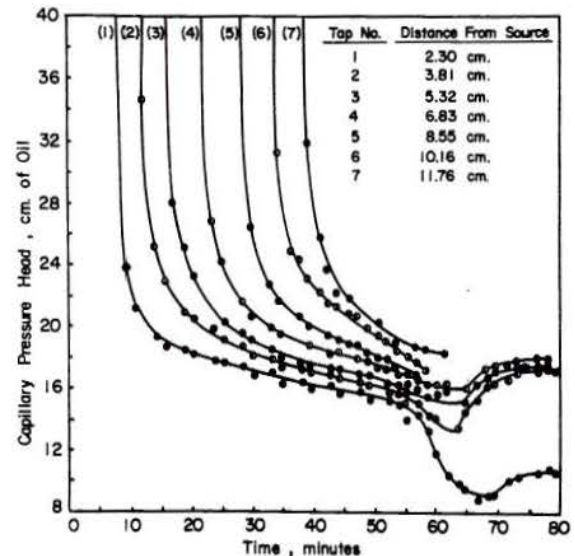


FIGURE 26 - Capillary pressure head as a function of time and position during constant rate infiltration.

The progress of the "wetting front" is readily observed from this figure. An important feature of the curves in this graph is the rapid decrease in the capillary pressure when the "wetting front" reaches a particular point followed by a much slower decline. It is noticed that after the wetting front has passed, the rate of decline of capillary pressure is least for points nearest the upper surface. It is not possible to measure the capillary pressure immediately at the surface, but it can be concluded that, after the initial wetting, the rate of decline of capillary pressure at the surface was less than that measured at tap (1). The significance of this observation is that the capillary pressure at the surface of the soil approaches the capillary pressure at which ponding occurs almost asymptotically. Therefore, the time at which ponding occurs is very sensitive to the properties of the porous medium. The properties of the porous medium at the surface are especially important.

Attempts to reproduce the ponding time observed in a particular experiment verified this conclusion.

In view of the difficulty experienced in reproducing the experimental data, no attempt was made to make numerical comparisons between experimental data and the theoretical developments for the constant rate boundary conditions. The theoretical results are useful because the factors affecting the phenomenon can be determined easily; at least in a qualitative sense. Figure 27 shows an example of the predicted variation in the capillary pressure at the surface. Note that, qualitatively, this curve agrees with the measured curves in Figure 25.

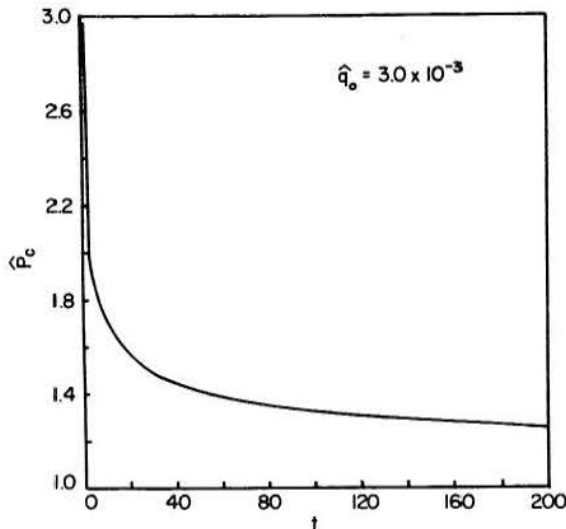


FIGURE 27 - Calculated capillary pressure as a function of time at the surface.

Figure 28 shows how the ponding time varies with the application rate. For this example, scaled application rates less than  $2.4 \times 10^{-3}$  will not result in ponding. It is observed that the ponding time becomes very sensitive to the infiltration rate for rates near  $2.4 \times 10^{-3}$ . This trend was verified experimentally by determining the ponding time at various application rates. The results are shown in Table 1.

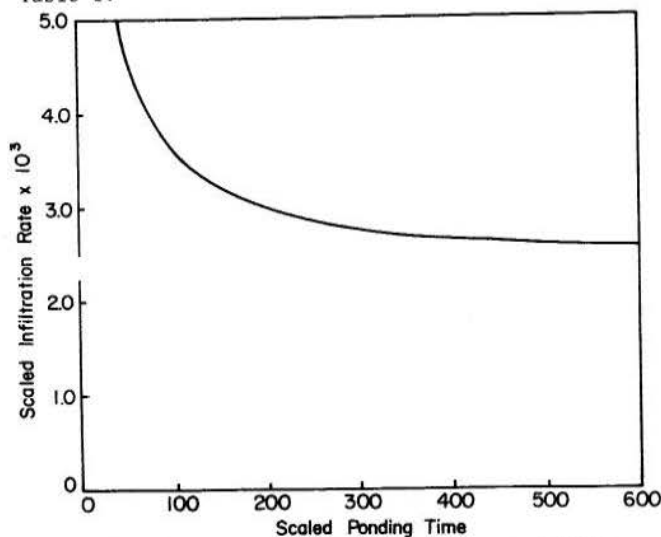


FIGURE 28 - Calculated relationship between infiltration rate and ponding time.

TABLE 1 - Observed Dependence of Ponding Time on Infiltration Rate

Infiltration Rate cm/min.	Ponding Time min.
0.154	35
0.103	62
0.076	218
0.074	---

From the data in Figure 26, plots of the capillary pressure profiles at various times were constructed. These are shown in Figure 29. From these curves, it is observed that to some degree of approximation, different values of capillary pressure propagate with the same velocity at any particular time. It is on this approximation that equations (120) and (123) are based.

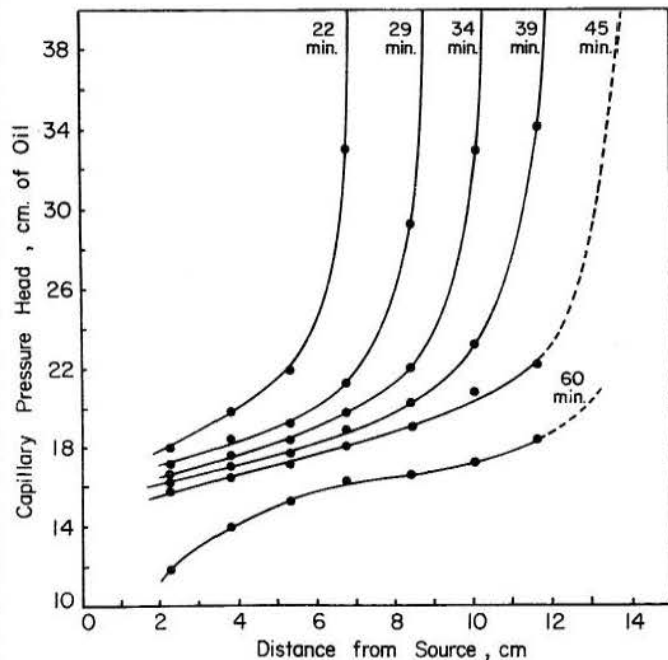


FIGURE 29 - Measured capillary pressure profiles during constant rate infiltration.

The ponding time for the experiment from which the data in Figures 26 and 29 were taken was observed to be 62 minutes from the time of application of the constant rate. The capillary pressure at tap 1 began to decrease sharply at about this time. This is explained by the fact that, just prior to ponding, the saturation at points near the surface was near  $\hat{S} = 1.0$ . A further increase in  $S$  resulted in a sharp decline in capillary pressure because  $P_c$  decreases very rapidly with increasing saturation in this range (see Figure 12). The increase in saturation beyond the saturation at which  $E(S)$  reaches a maximum (see the discussion following the derivation of equation (123)) occurs because the air is compressible. It was observed that the counterflow of air ceased when ponding occurred and the air was compressed until the pressure increased to a value at which it again escaped from the top of the column.

CONCLUSIONS AND RECOMMENDATIONS

The phenomenon of one-dimensional flow of two immiscible fluids in porous media was studied both theoretically and experimentally, with particular emphasis on the infiltration problem. The theoretical work was based on a differential equation derived by combining Darcy's law for both fluids with the equation of mass conservation. Experiments used in the study were designed to simulate field situations in which the resistance to flow of the displaced air significantly affects the flow of the liquid.

The following conclusions were drawn as a result of this study.

- 1) The construction of similar physical systems in which the flow phenomenon is that of an incompressible wetting fluid displacing a compressible non-wetting fluid is impractical in all but a few simple cases. Five criteria for the construction of similar physical systems were recognized. These are:

- a) The overall geometry of the two systems must be such that corresponding dimensions form identical ratios to  $P_0/\rho_w g$ .  $P_0$  is the scale factor for pressure.
- b) The theory implicitly required the same orientation with respect to the gravitational field.
- c) Initial and boundary conditions must be identical when expressed in terms of the scaled variables.
- d) The viscosity ratio  $\mu_a/\mu_w$  must be identical in both systems.
- e) The functions of scaled variables listed below must be identical;

$$\begin{aligned} k_{ra} &= k_{ra}(\hat{S}) \\ k_{rw} &= k_{rw}(\hat{S}) \\ \hat{P}_c &= \hat{P}_c(\hat{S}) \\ \hat{\rho}_a &= \hat{\rho}_a(\hat{P}_a) \end{aligned}$$

- 2) The differential equation describing one-dimensional horizontal displacement of an incompressible non-wetting fluid by an incompressible wetting fluid in a semi-infinite medium subject to the conditions of constant saturation at  $x = 0$  and uniform initial saturation can be reduced to an ordinary differential equation by the Boltzman similarity transformation.
- 3) Theoretically, a zone in which the capillary pressure is less than that value at which the air phase becomes discontinuous (a zone in which  $S = 1.0$ ) does not develop in the porous medium. This is true even under ponded liquid conditions. This conclusion implies that the governing equations (expressed with saturation as the dependent variable) are valid even under conditions of ponded liquid.

- 4) The saturation profile contains an inflection point near  $\hat{S} = 1.0$  which is the result of the large resistance to flow of the air at these saturations. This is in agreement with the Buckley-Leverett profile obtained by neglecting capillary pressure gradients (Brustkern and Morel-Seytoux (14)).
- 5) The limiting value approached by the infiltration rate (scaled) in a semi-infinite medium is:

$$\lim_{t \rightarrow \infty} \hat{q}_0 = \lim_{S \rightarrow 1.0} \frac{E(\hat{S})}{F_{w1}(\hat{S}) - f_w(\hat{S})}$$

For the case in which  $dk_{ra}/d\hat{S}|_{\hat{S}=1.0} \neq 0$  the above limit is equal to  $\mu_a k_{rw}(1)/\mu_w$  which is the scaled value of the hydraulic conductivity at  $\hat{S} = 1.0$ . If  $k'_{ra}(1.0) = 0$  it is believed that the limiting value of  $\hat{q}_0$  is somewhat less than  $\mu_a k_{rw}(1)/\mu_w$ , although this was not definitely proven.

- 6) Calculation of the infiltration into Poudre sand from equation (108) agrees well with experiment. This equation overestimates the effect of gravitational forces to an unknown degree.
- 7) The rate of infiltration into columns constructed so that the air cannot escape from the bottom is significantly slowed by the resistance to the flow of the air under certain conditions. The infiltration rate is, initially, very high but decreases rapidly to a minimum value well below the hydraulic conductivity at  $\hat{S} = 1.0$ . The pressure in the air is increased because it is compressed by the infiltrating liquid. Air begins to escape from the top of the column when the capillary pressure at the surface has reached some threshold value. The value of the capillary pressure at which air begins to escape is considerably higher than would be predicted from the primary imbibition capillary pressure-saturation curve. These conclusions are in agreement with those of Young and Peck (36).  
When air begins to escape from the column, the infiltration rate increases. In the case of Poudre sand, the infiltration rate increased to a peak and again declined to a value somewhat below the hydraulic conductivity at  $\hat{S} = 1.0$ . It is believed that the increase in the infiltration rate to values higher than the hydraulic conductivity at  $\hat{S} = 1.0$  is the result of a disturbance in the Poudre sand near the surface caused by the escaping air.
- 8) Theoretical results for the case of constant rate infiltration with air counterflow show that ponding will occur if the scaled value of the application rate exceeds the maximum value of  $E(\hat{S})$ .

- 9) Both theoretical and experimental results show that the capillary pressure (or saturation) at the surface approaches the value at which ponding occurs at a rate which depends upon the application rate. The critical value of capillary pressure (or saturation) is approached almost asymptotically in time when the scaled application rate is only slightly larger than the maximum value of  $E(S)$ . Therefore ponding time is large. For larger application rates, ponding will occur more quickly. The relative magnitude of these changes can be predicted from the theory. The theory can be used (in a qualitative sense) to determine how the ponding time depends on the hydraulic properties of the porous medium.

Several aspects of the work in this paper are incomplete and require further study. The degree to

which  $F_{w1}$  depends upon  $k_{ra}(\hat{S})$  near  $\hat{S} = 1.0$  should be studied in more detail. In conjunction with such a study, an experiment should be designed to investigate the shape of the saturation profile of values of  $\hat{S}$  near 1.0.

The degree to which gravitational forces are overestimated by equation (94) and (108) should be determined. This could be accomplished by comparisons with other solutions.

The solution procedure for problems of infiltration into finite media is not sufficiently general to predict all of the important aspects of this phenomenon. Efforts should be made to either extend the present method or develop a new procedure.

Finally, a simple routine method for measuring the relative permeability to air as a function of saturation for unconsolidated materials should be developed.

REFERENCES

1. Adrian, D. D. and Franzini, J. B., "Impedance to infiltration by pressure build-up ahead of the wetting front", *J. Geophys. Res.*, Vol. 71, No. 24, 5857-5863, 1966.
2. Ames, W. S., Non-linear partial differential equation in engineering, Academic Press, New York, 1965.
3. Brooks, R. H. and Corey, A. T., "Hydraulic properties of porous media," Colorado State University, Fort Collins, Colorado Hydrology Paper No. 3, March 1964.
4. Brustkern, R. L. and Morel-Seytoux, H. J., "Analytical treatment of two-phase infiltration," *Proc. of ASCE, Jour. of Hyd. Division*, Vol. 96, No. HY12, 2535-2548, Dec. 1970.
5. Buckley, S. E. and Leverett, M. C., "Mechanism of fluid displacement in sands," *Trans. AIME*, Vol. 146, 107-116, 1942.
6. Childs, E. C., The physical basis of soil water phenomena, John Wiley and Sons Ltd., 1969.
7. Corey, A. T., Unpublished study of techniques for measuring the relationship between capillary pressure and saturation.
8. Corey, G. L., Corey, A. T., and Brooks, R. H., "Similitude for non-steady drainage of partially saturated soils," Colorado State University, Fort Collins, Colorado, Hydrology Paper No. 9, August 1965.
9. Dicker, D., "Transient free surface flow in porous media," in Flow through porous media, DeWiest, R. J. M., ed., Academic Press, New York, 1969.
10. Free, J. R. and Palmer, V. J., "Relationship of infiltration, air movement, and pore size in graded silica sand," *Soil Sci. Soc. of Amer. Proc.*, Vol. 5, 390-398, 1940.
11. Green, W. H. and Ampt, G. A., "Studies in soil physics: 1. The flow of air and water through soils," *J. Agr. Sci.*, Vol. 4, 1-24, 1911.
12. Hanks, R. J. and Bowers, S. A., "Numerical solution of the moisture flow equation for infiltration into layered soils," *Soil Sci. Soc. of Amer. Proc.*, Vol. 26, No. 6, 530-534, 1962.
13. Horton, R. E., "An approach toward physical interpretation of infiltration capacity," *Soil Sci. Soc. of Amer. Proc.*, Vol. 5, 399-417, 1940.
14. McWhorter, D. B. and Corey, A. T., "Similitude for flow of two fluids in porous media," *Proc. Intern. Hydrology Symposium*, Vol. 1 Fort Collins, Colorado, September 1967.
15. Morel-Seytoux, H. J., "Flow of immiscible liquids in porous media," in Flow through porous media, DeWiest, R. J. M., ed., Academic Press, New York, 1969.
16. Parlange, J. Y., "Theory of water-movement in soils, 1: Part 2 - One-dimensional infiltration," *Soil Sci.*, March 1971.
17. Peck, A. J., "Moisture profile development and air compression during water uptake by bounded porous bodies, 2: Horizontal columns," *Soil Sci.*, Vol. 100, No. 1, 44-51, 1965.
18. Peck, A. J., "Moisture profile development and air compression during water uptake by bounded porous bodies, 3: Vertical columns," *Soil Sci.*, Vol. 100, No. 1, 44-51, 1965.
19. Philip, J. R., "The theory of infiltration: 1. The infiltration equation and its solution," *Soil Sci.*, Vol. 83, 345-357, 1957.
20. Philip, J. R., "The theory of infiltration: 2. The profile at infinity," *Soil Sci.*, Vol. 83, 435-448, 1957.
21. Philip, J. R., "The theory of infiltration: 3. Moisture profiles and relation to experiment," *Soil Sci.*, Vol. 84, 163-177, 1957.
22. Philip, J. R., "The theory of infiltration: 4. Sorptivity and algebraic infiltration equation," *Soil Sci.*, Vol. 84, 257-264, 1957.
23. Philip, J. R., "The theory of infiltration: 5. The influence of initial moisture content," *Soil Sci.*, Vol. 84, 329-339, 1957.
24. Philip, J. R., "The theory of infiltration: 6. Effect of water depth over soil," *Soil Sci.*, Vol. 85, 278-286, 1958.
25. Philip, J. R., "The theory of infiltration: 7.," *Soil Sci.*, Vol. 85, 333-337, 1959.
26. Phuc, Le Van, "General one-dimensional model for infiltration," Unpublished M.S. Thesis, Colorado State University, Fort Collins, Colorado, 1969.
27. Richards, L. A., "Capillary conduction of liquids through porous mediums," *Physics*, Vol. 1, 318-333, 1931.
28. Rubin, J. and Steinhardt, R., "Soil water relations during rain infiltration: 1. Theory," *Soil Sci. Soc. of Amer. Proc.*, Vol. 27, No. 3, 246-251, 1963.
29. Scott, V. H. and Corey, A. T., "Pressure distribution during steady flow in unsaturated sands," *Soil Sci. Soc. of Amer. Proc.*, Vol. 27, No. 3, 246-251, 1963.

30. Skaggs, R. W., Monke, E. J., and Huggins, L. F., "An approximate method of determining the hydraulic conductivity function of unsaturated soil," Purdue University, Lafayette, Indiana, Tech. Rep. No. 11, June 1970.
31. Smith R. E., "Mathematical simulation of infiltrating watersheds," Unpublished Ph.D. dissertation, Colorado State University, Fort Collins, Colorado 1970.
32. Whisler, F. D. and Klute, A., "The numerical analysis of infiltration considering hysteresis, into a vertical soil column at equilibrium under gravity," Soil Sci. Soc. Amer. Proc., Vol. 29, No. 5, 489-494, 1965.
33. Whisler, F. D. and Klute, A., "Rainfall infiltration into a vertical soil column," Trans. of ASAE, Vol. 10, No. 3, 391-395, 1967.
34. White, N. F., "The desaturation of porous media," Unpublished Ph.D. dissertation, Colorado State University, Fort Collins, Colorado 1968.
35. Wilson, L. G. and Luthin, J. N., "Effect of air flow ahead of the wetting front on infiltration," Soil Sci., Vol. 96, 136-143, 1963.
36. Youngs, E. G. and Peck, A. J., "Moisture profile development and air compression during water uptake by bounded porous bodies: 1. Theoretical introduction," Soil Sci., Vol. 98, 280-294, 1964.

APPENDIX A

HYDRAULIC PROPERTIES OF POROUS MEDIA

TABLE A-1 CAPILLARY PRESSURE - RELATIVE PERMEABILITY SATURATION DATA FOR POUFRE SAND

Drainage			Imbibition		
$P_c/\rho g$	$k_{rw}$	S	$P_c/\rho g$	$k_{rw}$	S
cm			cm		
23.0	1.000	1.00	73.6	0.001	0.32
29.3	1.000	1.02	56.8	0.004	0.38
33.7	1.000	1.01	50.7	0.006	0.40
36.8	0.904	1.00	45.0	0.013	0.44
39.1	0.750	0.97	38.9	0.036	0.47
40.8	0.578	0.90	34.6	0.096	0.62
42.9	0.422	0.87	32.0	0.118	0.64
45.7	0.240	0.78	28.9	0.204	0.72
48.3	0.143	0.68	25.6	0.362	0.81
50.8	0.094	0.61	19.0	0.690	0.89
56.4	0.036	0.51	12.7	0.800	0.91
59.9	0.026	0.47	7.2	0.816	0.90
63.3	0.016	0.44			
66.3	0.010	0.42			
75.9	0.003	0.35			
84.9	0.001	0.29			

$K = 2.52 \times 10^{-8} \text{ cm}^2, \phi = 0.396$

TABLE A-2 RELATIVE PERMEABILITY - SATURATION DATA FOR BEREA SANDSTONE - IMBIBITION

$k_{ra}$	S	$k_{rw}$	S
1.000	0.0	0.002*	0.40
0.986	0.079	0.016*	0.50
0.943	0.148	0.154	0.648
0.806	0.260	0.237	0.715
0.669	0.325	0.262	0.750
0.566	0.377	0.290	0.761
0.457	0.419	0.320	0.770
0.347	0.460	0.353	0.776
0.169	0.539		
0.090	0.574	0.400	0.780
0.051	0.605		
0.028	0.619		
0.021	0.628		
0.004	0.651		

\*From drainage curve  
 $K = 0.384 \times 10^{-8} \text{ cm}^2$   
 $\phi = 0.201$

TABLE A-3 CAPILLARY PRESSURE - SATURATION DATA FOR BEREA SANDSTONE

Drainage		Imbibition	
$P_c/\rho g$	S	$P_c/\rho g$	S
cm		cm	
10.0	1.000	164.5	0.279
20.0	1.000	149.2	0.293
33.5	1.000	141.0	0.298
40.0	0.978	124.5	0.305
48.0	0.977	108.3	0.321
49.5	0.976	93.9	0.342
51.0	0.940	81.6	0.356
53.0	0.896	68.4	0.395
54.5	0.859	58.2	0.428
58.0	0.767	49.2	0.474
60.0	0.720	39.3	0.549
62.0	0.674	33.3	0.614
70.6	0.549	29.3	0.674
75.8	0.502	23.6	0.712
80.8	0.470	19.1	0.735
85.6	0.442	12.2	0.758
93.5	0.405	9.6	0.763
103.8	0.377		
113.3	0.342		
128.3	0.326		
148.3	0.293		
178.4	0.274		

APPENDIX B

INFILTRATION DATA FOR SIMULATED SEMI-INFINITE COLUMNS

TABLE B-1 INFILTRATION DATA FOR SIMULATED SEMI-INFINITE COLUMN OF POUFRE SAND

Cumulative Infiltration cm	Infiltration Rate cm/min	Time Min
0.55	1.58	0.25
0.79	0.86	0.50
0.98	0.65	0.75
1.12	0.56	1.00
1.25	0.52	1.25
1.77	0.42	2.50
1.95	0.35	3.00
2.13	0.32	3.50
2.27	0.27	4.00
2.53	0.26	5.00
2.79	0.24	6.00
3.02	0.22	7.00
3.23	0.22	8.00
3.50	0.21	9.00
3.65	0.20	10.00
3.85	0.20	11.00
4.23	0.17	13.00
4.40	0.17	14.00
4.57	0.17	15.00
4.74	0.16	16.00
5.07	0.16	18.00
5.37	0.15	20.00
5.66	0.14	22.00
5.94	0.14	24.00
6.21	0.14	26.00
6.49	0.13	28.00
6.74	0.13	30.00
7.42	0.13	35.00
8.00	0.11	40.00
8.55	0.11	45.00

Column Area =  $7.892 \text{ cm}^2$ ,  $\phi = 0.396$ ,  $K = 2.41 \times 10^{-8} \text{ cm}^2$   
 Poned liquid depth = 1.6 cm  
 Temperature = 23.4°C.

TABLE B-2 INFILTRATION DATA FOR SIMULATED SEMI-INFINITE COLUMN OF BEREA SANDSTONE

Cumulative Infiltration cm	Infiltration Rate cm/min	Time Min
0.048	0.147	0.25
0.073	0.090	0.50
0.093	0.066	0.75
0.106	0.052	1.00
0.133	0.044	1.50
0.150	0.039	2.00
0.172	0.034	2.50
0.184	0.028	3.00
0.215	0.028	4.00
0.241	0.024	5.00
0.263	0.022	6.00
0.284	0.021	7.00
0.306	0.020	8.00
0.323	0.018	9.00
0.341	0.016	10.00
0.371	0.015	12.00
0.401	0.015	14.00
0.429	0.014	16.00
0.455	0.012	18.00
0.479	0.012	20.00
0.505	0.012	22.00
0.529	0.012	24.00
0.553	0.011	26.00
0.575	0.010	28.00
0.594	0.010	30.00
0.646	0.010	35.00
0.696	0.009	40.00
0.739	0.009	45.00
0.783	0.009	50.00
0.826	0.009	55.00
0.868	0.008	60.00

Column Area =  $20.65 \text{ cm}^2$ ,  $\phi = 0.201$ ,  $K = 0.384 \times 10^{-8} \text{ cm}^2$   
 Poned Liquid Depth = 0.8 cm  
 Temperature = 22.5°C.

APPENDIX C

INFILTRATION DATA FOR FINITE COLUMNS

TABLE C-1 INFILTRATION DATA FOR COLUMN OF POUFRE SAND  
990 cm Equivalent Length

Cumulative Infiltration cm.	Infiltration Rate cm/Min	Air Press. Head cm. of oil	Time Min.
0	----	0	0
.48	1.43	.8	0.25
.71	0.81	1.1	0.50
1.04	0.58	1.5	1.00
1.17	0.47	1.7	1.25
1.28	0.41	1.9	1.50
1.37	0.43	2.0	1.75
1.50	0.39	2.1	2.00
1.57	0.30	----	2.25
1.65	0.31	----	2.50
1.72	0.36	----	2.75
1.82	0.34	----	3.00
1.96	0.26	----	3.50
2.09	0.25	----	4.00
2.22	0.24	----	4.50
2.33	0.22	----	5.00
2.45	0.20	----	5.50
2.53	0.19	----	6.00
2.65	0.21	----	6.50
2.75	0.20	----	7.00
2.84	0.16	----	7.50
2.90	0.16	----	8.00
2.99	0.16	----	8.50
3.07	0.15	----	9.00
3.14	0.15	----	9.50
3.21	0.16	9.3	10.00
3.29	0.17	----	10.50
3.38	0.15	10.0	11.00
3.45	0.12	10.2	11.50
3.51	0.12	10.5	12.00
3.62	0.13	10.8	13.00
3.75	0.13	11.3	14.00
3.88	0.13	11.5	15.00
4.00	0.12	12.0	16.00
4.22	0.11	12.5	18.00
4.33	0.11	13.0	19.00
4.48	0.11	13.3	20.00
4.65	0.11	14.0	22.00
4.88	0.11	14.5	24.00
5.03	0.10	15.2	26.00
5.22	0.09	15.8	28.00
5.37	0.08	16.3	30.00
5.78	0.08	17.5	35.00
6.17	0.08	18.8	40.00
6.51	0.07	19.8	45.00
6.84	0.07	21.0	50.00
7.18	0.06	22.3	56.00
7.41	0.06	23.0	60.00
7.70	0.06	24.0	65.00
7.89	0.05	24.5	70.00
8.20	0.05	25.2	75.00
8.43	0.05	26.0	80.00

Atmospheric Pressure = 1182 cm. of oil  
Temperature = 23.0°C

TABLE C-2 INFILTRATION DATA FOR COLUMN OF POUFRE SAND  
670 cm Equivalent Length

Cumulative Infiltration cm.	Infiltration Rate cm/Min.	Air Press. Head cm. of oil	Time Min.
0.0	---	0	0.00
.50	1.47	1.7	0.25
.74	0.84	2.8	0.50
.91	0.61	3.5	0.75
1.04	0.51	4.0	1.00
1.17	0.48	4.5	1.25
1.28	0.46	4.9	1.50
1.39	0.41	5.1	1.75
1.48	0.37	5.5	2.00
1.67	0.30	6.3	2.50
1.79	0.24	6.9	3.00
1.91	0.24	7.5	3.50
2.02	0.23	8.0	4.00
2.14	0.20	8.3	4.50
2.23	0.19	8.6	5.00
2.33	0.20	9.1	5.50
2.52	0.15	9.8	6.50
2.57	0.15	10.1	7.00
2.67	0.18	10.6	7.50
2.75	0.15	11.0	8.00
2.83	0.14	11.3	8.50
2.89	0.14	11.5	9.00
2.96	0.13	11.9	9.50
3.02	0.12	12.3	10.00
3.15	0.14	12.9	11.00
3.29	0.12	13.3	12.00
3.39	0.11	13.5	13.00
3.51	0.11	14.0	14.00
3.62	0.11	14.6	15.00
3.72	0.10	15.1	16.00
3.92	0.10	16.1	18.00
4.40	0.09	17.5	22.00
4.45	0.05	18.4	24.00
4.59	0.08	19.0	26.00
4.73	0.07	19.3	28.00
4.85	0.06	20.0	30.00
5.14	0.05	21.6	35.00
5.41	0.04	22.8	40.00
5.65	0.05	24.5	46.00
5.11	0.03	25.8	55.00
6.34	0.03	26.8	63.00
6.41	0.03	27.2	65.00
6.55	0.04	28.4	70.00
6.73	0.03	28.5	75.00
6.85	0.03	29.5	80.00
7.01	0.03	30.0	86.00
7.11	0.02	30.5	90.00
7.22	0.02	31.0	95.00
7.33	0.02	31.5	100.00
7.47	0.02	31.6	106.00
7.56	0.02	32.0	110.00
7.65	0.02	32.5	115.00
7.75	0.02	33.0	120.00

Atmospheric Pressure = 1106 cm. of oil  
Temperature = 22.9°C.

TABLE C-3 INFILTRATION DATA FOR COLUMN OF POUFRE SAND  
393 cm Equivalent Length

Cumulative Infiltration cm	Infiltration Rate cm/min	Air Press. Head cm. of oil	Time Min
0.00	---		0.0
0.56	1.54	2.5	0.25
0.77	0.71	4.3	0.50
0.91	0.56	---	0.75
1.05	0.48	6.5	1.00
1.15	0.43	---	1.25
1.27	0.41	8.0	1.50
1.36	0.33	---	1.75
1.43	0.30	9.5	2.00
1.58	0.25	10.6	2.50
1.69	0.22	11.5	3.00
1.80	0.22	12.4	3.50
1.90	0.20	13.0	4.00
2.00	0.18	13.8	4.50
2.08	0.14	14.5	5.00
2.14	0.15	15.0	5.55
2.23	0.14	15.5	6.00
2.28	0.14	16.1	6.50
2.37	0.15	16.6	7.00
2.43	0.11	17.0	7.50
2.48	0.10	17.5	8.00
2.58	0.10	18.2	9.00
2.69	0.10	19.0	10.00
2.77	0.09	19.6	11.00
2.86	0.08	20.4	12.00
2.94	0.08	20.9	13.00
3.02	0.07	21.4	14.00
3.10	0.07	---	15.00
3.15	0.06	22.5	16.00
3.28	0.06	23.3	18.00
3.40	0.05	24.0	20.00
3.50	0.05	---	22.00
3.59	0.04	25.2	24.00
3.67	0.04	25.6	26.00
3.74	0.04	---	28.00
3.83	0.04	26.5	30.00
3.90	0.04	---	32.00
4.02	0.03	27.4	35.00
4.16	0.03	28.2	40.00
4.29	0.03	28.8	45.00
4.43	0.03	29.0	50.00
4.56	0.03	29.2	55.00
4.68	0.02	29.7	60.00
4.79	0.02	30.0	65.00
4.89	0.02	30.1	70.00
5.00	0.02	30.2	75.00
5.21	0.02	30.5	85.00
5.30	0.02	30.5	90.00
5.40	0.02	30.5	95.00
5.57	0.03	30.5	106.00
5.78	0.02	30.6	110.00

Atmospheric Pressure = 1098 cm. of oil  
Temperature = 22.8°C  
\*Possible air leak

TABLE C-4 INFILTRATION DATA FOR COLUMN OF POUFRE SAND  
233 cm Equivalent Length

Cumulative Infiltration cm.	Infiltration Rate cm/Min	Air Press. Head cm. of oil	Time Min.
0	----	0	0
0.60	1.40	----	0.25
0.70	0.46	----	0.50
0.82	0.48	----	0.75
0.94	0.40	----	1.00
1.03	0.30	11.5	1.25
1.09	0.25	----	1.50
1.15	0.25	----	1.75
1.22	0.24	----	2.00
1.33	0.20	16.0	2.50
1.42	0.15	----	3.00
1.48	0.14	----	3.50
1.56	0.13	----	4.00
1.61	0.10	----	4.50
1.66	0.09	21.0	5.00
1.70	0.09	----	5.50
1.75	0.09	----	6.00
1.82	0.07	----	7.00
----	----	23.8	7.50
1.89	0.06	----	8.00
1.95	0.05	----	9.00
2.00	0.04	26.0	10.00
2.04	0.05	----	11.00
2.09	0.04	----	12.00
2.15	0.03	----	14.00
----	----	28.6	15.00
2.20	0.03	----	16.00
2.25	0.03	----	18.00
2.30	0.02	30.6	20.00
2.34	0.02	----	22.00
2.39	0.02	31.8	25.00
2.46	0.01	33.0	30.00
2.50	0.02	----	33.00
2.51	0.04	----	33.50
2.53	0.04	----	34.00
2.55	0.03	----	34.50
2.57	0.05	30.0	35.00
2.61	0.06	----	36.00
2.64	0.51	----	36.50
2.66	0.51	----	37.00
2.69	0.08	23.5	37.50
2.74	0.10	----	38.00
2.79	0.09	----	38.50
2.83	0.09	----	39.00
2.88	0.14	----	39.50
2.91	0.13	21.5	40.00
2.99	0.07	----	41.00
3.05	0.08	----	42.00
3.14	0.08	----	43.00
3.22	0.08	----	44.00
3.29	0.07	21.8	45.00
3.36	0.06	----	46.00
3.42	0.06	----	47.00
3.48	0.06	----	48.00
3.61	0.06	23.0	50.00
3.88	0.05	----	55.00
4.13	0.05	24.3	60.00
4.37	0.05	----	65.00
4.60	0.04	24.5	70.00
5.04	0.04	24.7	80.00
5.46	0.04	25.5	90.00
5.87	0.04	----	100.00
6.28	0.04	----	110.00
6.49	0.04	----	115.00
6.68	0.04	----	120.00

Atmospheric Pressure = 1206 cm. of oil  
Temperature = 23.0°C

TABLE C-5 INFILTRATION DATA FOR COLUMN OF POUFRE SAND  
185 cm Equivalent Length

Cumulative Infiltration cm.	Infiltration Rate cm/Min.	Air Press. Head cm. of oil	Time Min.
		0	0.00
0.57	1.47	-	0.25
0.73	0.46	10	0.50
0.80	0.53	-	0.75
1.00	0.58	-	1.00
1.09	0.28	15.1	1.25
1.14	0.25	----	1.50
1.22	0.23	----	1.75
1.25	0.18	----	2.00
1.36	0.19	20.4	2.50
1.44	0.11	----	3.00
1.47	0.06	----	3.50
1.51	0.09	----	4.00
1.56	0.06	----	4.50
1.57	0.05	25.0	5.00
1.65	0.06	----	6.00
1.69	0.04	----	7.00
----	----	27.2	7.50
1.74	0.04	----	8.00
1.77	0.03	----	9.00
1.80	0.03	29.0	10.00
1.85	0.02	30.2	12.00
1.89	0.02	----	14.00
----	----	31.3	15.00
1.93	0.03	----	16.00
----	----	31.5	16.50
1.96	0.06	27.5	17.00
----	----	25.0	17.50
2.05	0.10	----	18.00
----	----	22.0	18.75
2.15	0.11	----	19.00
2.27	0.10	20.7	20.00
2.36	0.09	20.7	21.00
2.45	0.09	22.0	22.00
2.53	0.08	----	23.00
2.61	0.06	----	24.00
2.67	0.08	22.8	25.00
2.75	0.05	----	26.00
2.80	0.06	----	27.00
2.86	0.07	----	28.00
3.00	0.06	23.4	30.00
3.32	0.06	----	35.00
3.62	0.06	23.6	40.00
----	0.06	25.2	50.00
4.37	0.05	----	55.00
4.57	0.04	26.0	60.00
5.07	0.04	----	70.00
----	----	26.4	73.00
5.13	0.04	----	75.00
5.30	0.04	27.0	80.00
5.47	0.03	----	85.00
5.64	0.03	27.3	90.00
5.79	0.03	----	95.00
5.97	0.03	27.3	100.00
6.12	0.03	----	105.00
6.27	0.03	27.3	110.00
6.45	0.03	----	115.00
6.60	0.03	27.3	120.00

Atmospheric Pressure = 1181 cm of oil  
Temperature = 23.0°C

TABLE C-6 INFILTRATION DATA FOR COLUMN OF BERE A  
SANDSTONE  
17.4 cm Equivalent Length

Cumulative Infiltration cm.	Air Press. Head cm. of oil	Time Min.
0.069	22.4	1.0
0.090	30.2	2.0
0.102	34.6	3.0
0.112	37.5	4.0
0.117	----	4.5
0.121	39.9	5.0
0.127	----	6.0
0.131	43.4	7.0
0.136	----	8.0
0.138	----	8.5
0.138	45.3	9.0
----	45.7	10.0
0.145	45.7	11.0
0.149	45.7	12.0
0.158	45.4	14.0
0.166	45.4	16.0
0.173	45.2	18.0
0.182	45.3	20.0
0.188	45.2	22.0
0.199	44.5	25.0
0.216	44.5	30.0
0.234	43.6	35.0

Atmospheric Pressure = 1149 cm. of oil  
Temperature = 22.8°C

APPENDIX D

AIR PRESSURE BUILD-UP DATA FOR COLUMNS OF POUFRE SAND

TABLE D-1 AIR PRESSURE BUILD-UP IN COLUMNS OF POUFRE SAND  
WITH OPEN LOWER END

50.8 cm column		25.4 cm column	
Time Sec	Air Press. Head cm of oil	Time Sec	Air Press. Head cm of oil
6	9.6	3.5	7.2
11	7.9	4	7.1
16	6.5	9	4.5
21	5.5	14	3.4
26	4.9	19	2.8
31	4.5	24	2.4
36	4.1	29	2.1
41	3.8	34	2.0
46	3.6	39	1.8
51	3.4	44	1.8
56	3.2	49	1.6
61	3.1	54	1.6
66	3.0	59	1.6
71	2.8	64	1.5
76	2.7	69	1.5
81	2.6		
86	2.6		
91	2.5		
96	2.4		
101	2.3		
121	2.2		
141	2.1		
161	2.0		

APPENDIX E

CONSTANT RATE INFILTRATION DATA

TABLE E-1 TAP 1 - 2.30 cm FROM SOURCE

Time Min.	Oil Press. Head cm. of oil	Air Press. Head cm. of oil	Capillary Press. Head cm. of oil
1.3	-134.1	0	134.1
2.3	-110.7	0	110.7
4.5	-104.8	0.2	105.0
6.1	- 95.6	-0.1	95.5
7.1	- 54.9	-0.1	54.8
9.3	- 23.7	0.1	23.8
10.9	- 21.4	-0.2	21.2
14.1	- 19.4	0	19.4
15.7	- 19.0	-0.3	18.7
18.9	- 18.5	0	18.5
20.5	- 18.2	0	18.2
23.7	- 17.7	0.1	17.8
25.3	- 17.6	0.1	17.7
28.5	- 17.3	0.1	17.4
30.1	- 17.0	-0.2	16.8
33.3	- 16.7	0.3	17.0
34.9	- 16.4	-0.2	16.2
38.1	- 16.1	0.2	16.3
39.7	- 16.0	-0.1	15.9
42.9	- 15.7	0.4	16.1
44.5	- 15.6	0	15.6
47.7	- 15.4	0.4	15.8
49.3	- 15.2	0.0	15.2
52.5	- 14.9	0.3	15.2
54.1	- 14.7	0.2	14.9
55.1	- 13.9	0.0	13.9
57.3	- 13.8	0.4	14.2
58.9	- 12.8	0.4	13.2
59.9	- 11.6	0.1	11.7
62.1	- 9.9	0.4	10.3
63.7	- 4.0	5.8	9.8
64.7	- 1.8	7.7	9.5
66.9	1.6	10.4	8.8
68.5	2.3	11.3	9.0
69.5	2.7	11.8	9.1
71.7	2.9	12.8	10.0
73.3	3.2	13.4	10.2
76.5	3.2	13.7	10.5
78.1	2.9	13.7	10.8
79.1	3.1	13.6	10.5

TABLE E-2 TAP 2 - 3.81 cm FROM SOURCE

Time Min	Oil Press. Head cm. of oil	Air Press. Head cm. of oil	Capillary Press. Head cm. of oil
1.2	-82.2	--	82.2
2.4	-78.5	0.1	78.6
4.4	-79.9	0.1	80.0
6.0	-79.4	-0.1	79.5
9.2	-79.9	0	79.9
10.8	-76.1	0	76.1
12.0	-34.9	-0.2	34.7
14.0	-25.2	0	25.2
15.6	-23.2	-0.3	22.9
18.8	-21.0	-0.1	20.9
20.4	-20.6	-0.1	20.5
23.6	-19.6	0.2	19.8
25.2	-19.2	-0.1	19.1
28.4	-18.6	0.1	18.7
30.0	-18.2	-0.1	18.1
33.2	-17.7	0.2	17.9
34.8	-17.3	0	17.3
38.0	-16.9	0.3	17.2
39.6	-16.7	0.3	17.0
42.8	-16.4	0.4	16.8
44.4	-16.2	0.4	16.6
47.6	-15.8	0.5	16.3
49.2	-15.6	0.5	16.1
52.4	-15.2	0.5	15.7
54.0	-14.9	0.7	15.6
55.2	-14.1	0.8	14.9
57.2	-13.8	1.2	15.0
58.8	-12.5	1.7	14.2
60.0	-11.4	2.6	14.0
62.0	- 9.6	5.4	15.0
63.6	- 4.6	8.8	13.4
64.8	- .1	14.3	14.4
66.8	2.3	17.5	15.2
68.4	3.1	19.2	16.1
69.6	3.6	19.9	16.3
71.6	3.6	20.2	16.6
73.2	3.7	20.7	17.0
76.4	3.8	20.9	17.1
78.0	3.7	20.9	17.2
79.2	3.7	20.8	17.1

\*Constant infiltration rate = 0.813 cm<sup>3</sup>/min.

TABLE E-3 TAP 3 - 5.32 cm FROM SOURCE

Time Min	Oil Press. Head cm. of oil	Air Press. Head cm. of oil	Press. Head cm. of oil
1.1	-155.0		155
2.5	-142.4	- 0.1	142.3
4.3	-139.9	0.1	140.0
5.9	-138.0	0.1	138.1
7.3	-130.5	- 0.3	130.2
10.7	-130.6	0.1	130.7
13.9	-121.8	- 0.1	121.7
15.5	-100.0	0	100.0
16.9	- 28.0	0	28.0
18.7	- 25.1	0	25.1
20.3	- 23.4	- .1	23.3
25.1	- 20.2	0	20.2
28.3	- 19.3	.3	19.6
29.9	- 18.8	.3	19.1
33.1	- 18.0	.5	18.5
34.7	- 17.5	.5	18.0
37.9	- 17.1	.6	17.7
39.5	- 16.8	.7	17.5
42.7	- 16.3	.9	17.2
44.3	- 16.2	1.0	17.2
47.5	- 15.8	1.1	16.9
49.1	- 15.6	1.2	16.8
52.3	- 15.0	1.3	16.3
53.9	- 14.7	1.5	16.2
55.3	- 14.0	1.8	15.8
57.1	- 13.4	2.6	16.0
58.7	- 12.0	3.4	15.4
60.1	- 11.0	4.6	15.6
61.9	- 9.1	6.7	15.8
64.9	.1	15.2	15.1
66.7	2.7	18.9	16.2
68.3	3.6	20.3	16.7
69.7	4.0	21.2	17.2
71.5	4.1	21.7	17.6
73.1	4.5	21.9	17.4
74.5	4.6	22.0	17.4
76.3	4.6	22.0	17.4
77.9	4.6	21.9	17.3

TABLE E-4 TAP 4 - 6.83 cm FROM SOURCE

Time Min	Oil Press. Head cm. of oil	Air Press. Head cm. of oil	Capillary Press. Head cm. of oil
1.0	-146.8	0	140.8
2.6	-136.6	-0.2	136.4
4.2	-134.3	-0.2	134.1
5.8	-133.3	0	133.3
7.4	-131.9	0	131.9
9.0	-131.8	0	131.8
10.6	-131.0	-0.3	130.7
12.2	-128.7	-0.1	128.6
13.8	-128.9	-0.1	128.8
15.4	-127.6	-0.1	127.5
18.6	-120.1	0	120.1
20.2	-119.1	0	119.1
21.8	- 55.2	-0.2	55.0
23.4	- 26.7	0.1	26.8
25.0	- 24.0	0.2	24.2
28.2	- 21.4	0.2	21.6
29.8	- 20.6	0	20.6
33.0	- 19.4	0.5	19.9
34.6	- 18.9	0.6	19.5
39.4	- 17.9	0.8	18.7
42.6	- 17.2	1.0	18.2
44.2	- 17.1	1.1	18.2
47.4	- 16.6	1.3	17.9
49.0	- 16.3	1.4	17.7
50.6	- 15.8	1.5	17.3
52.2	- 15.6	1.6	17.2
53.8	- 15.2	1.7	16.9
55.4	- 14.4	1.9	16.3
57.0	- 13.8	2.8	16.6
58.6	- 12.3	3.9	16.2
60.2	- 11.0	5.2	16.2
61.8	- 9.2	7.0	16.2
65	0.4	16.4	16.0
66.6	2.8	18.9	16.1
68.2	3.6	20.8	17.2
69.8	4.3	21.7	17.4
71.4	4.6	22.2	17.6
73.0	4.6	22.4	17.8
76.2	4.6	22.6	18.0
77.8	4.5	22.4	17.9

TABLE E-5 TAP 5 - 8.55 cm FROM SOURCE

Time Min	Oil Press. Head cm. of oil	Air Press. Head cm. of oil	Capillary Press. Head cm. of oil
0.9	-139.5	0	139.5
2.7	-135.2	0	135.2
4.1	-133.6	0.2	133.8
5.7	-133.0	0.1	133.1
7.5	-132.5	0	132.5
8.9	-131.9	0	131.9
10.5	-130.8	0	130.8
12.3	-130.1	-0.1	130.0
13.7	-129.2	-0.1	129.1
15.3	-128.4	-0.3	128.1
17.1	-126.6	-0.2	126.4
18.5	-126.0	-0.2	125.8
20.1	-124.9	0	124.9
21.9	-117.7	-0.2	117.5
23.3	-117.6	0.1	117.6
26.7	- 97.6	0.3	97.9
28.1	- 43.4	0.4	43.8
29.7	- 25.9	0.5	26.4
32.9	- 22.1	0.6	22.7
34.5	- 20.9	0.7	21.6
37.7	- 19.7	0.9	20.6
39.3	- 19.0	1.0	20.0
42.5	- 18.2	1.2	19.4
44.1	- 17.8	1.3	19.1
45.9	- 17.4	1.4	18.8
47.3	- 17.2	1.6	18.8
48.9	- 16.7	1.6	18.3
50.7	- 16.2	1.8	18.0
52.1	- 15.9	2.0	17.9
53.7	- 15.2	2.2	17.4
55.5	- 14.2	2.7	16.9
56.9	- 13.6	3.3	16.9
58.5	- 11.9	4.5	16.4
60.3	- 10.5	5.5	16.0
61.7	- 8.8	6.5	15.3
63.3	- 6.1	10.8	16.9
65.1	1.0	17.4	16.4
66.5	3.3	19.6	16.3
68.1	4.4	21.4	17.0
69.9	5.1	22.4	17.3
71.3	5.3	22.8	17.5
72.9	5.4	22.8	17.4
76.1	5.4	22.9	17.5
77.7	5.4	22.9	17.5

TABLE E-6 TAP 6 - 10.16 cm FROM SOURCE

Time Min	Oil Press. Head cm. of oil	Air Press. Head cm. of oil	Capillary Press. Head cm. of oil
0.8	-156.6	0	156.6
2.8	-149.1	0	149.1
4.0	-142.0	0	142.0
5.6	-137.0	-0.1	136.9
7.6	-137.4	-0.1	137.3
8.8	-132.0	-0.1	131.9
10.4	-128.0	-0.1	128.9
12.4	-129.1	-0.2	128.9
13.6	-124.0	-0.2	123.8
15.2	-120.9	-0.2	120.7
18.4	-118.4	-0.2	118.2
20.0	-115.2	-0.1	115.1
23.2	-112.7	-0.1	112.6
24.8	-109.6	0.1	109.7
26.8	-109.3	0.2	109.5
28.0	-105.5	0.2	105.7
29.6	-101.5	0.2	105.7
31.6	- 93.6	0.5	94.1
32.8	- 68.4	0.5	68.9
34.4	- 30.7	0.5	31.2
36.4	- 24.3	0.6	24.9
37.6	- 23.6	0.7	24.3
39.2	- 22.2	0.9	23.1
41.2	- 21.1	1.0	22.1
42.4	- 20.4	1.1	21.5
44.0	- 19.9	1.3	21.2
46.0	- 19.2	1.6	20.8
47.2	- 18.8	1.8	20.6
48.8	- 18.0	1.8	19.8
50.8	- 17.4	2.0	19.4
52.0	- 16.8	2.2	19.0
53.6	- 15.9	2.5	18.3
55.6	- 14.9	3.1	18.0
56.8	- 13.9	3.8	17.7
58.4	- 12.2	4.9	17.1
60.4	- 10.7	6.6	17.3
61.6	- 8.8	8.1	16.9
63.2	- 6.2	11.2	17.4
65.2	1.1	18.0	16.9
66.4	3.6	20.6	17.0
68.0	4.8	22.0	17.2
70.0	5.4	22.9	17.5
71.2	5.9	23.2	17.3
72.8	5.8	23.4	17.6
74.8	5.9	23.6	17.7
77.6	5.9	23.5	17.6

TABLE E-7 TAP 7 - 11.76 cm FROM SOURCE

Time Min	Oil Press. Head cm. of oil	Air Press. Head cm. of oil	Capillary Press. Head cm. of oil
0.7	-128.6	0	128.6
2.9	-129.6	0.1	129.7
3.9	-113.0	0.1	113.1
5.5	-103.6	-0.1	103.5
7.7	-111.2	-0.1	111.1
8.7	- 98.5	-0.1	98.4
10.3	- 91.9	-0.1	91.8
13.5	- 89.8	-0.2	89.6
15.1	- 85.2	-0.1	85.1
18.3	- 85.0	-0.2	84.8
19.9	- 80.8	-0.2	80.6
23.1	- 81.1	0	81.1
24.7	- 77.2	0.2	77.4
27.9	- 78.0	0.2	78.2
29.5	- 74.2	0.4	74.6
32.7	- 74.0	0.4	74.4
34.3	- 70.4	0.6	71.0
36.5	- 71.1	0.6	71.7
37.5	- 63.4	0.7	64.1
39.1	- 30.9	1.0	31.9
41.3	- 24.7	1.1	25.8
42.3	- 22.5	1.2	23.7
43.9	- 20.9	1.3	22.2
46.1	- 20.3	1.5	21.8
47.1	- 18.7	1.8	20.5
48.7	- 17.9	2.1	20.0
50.9	- 17.8	2.4	20.2
51.9	- 16.5	2.7	19.2
53.5	- 15.3	3.6	18.9
56.7	- 13.2	5.5	18.7
58.3	- 11.4	7.0	18.4
61.5	- 7.9	10.4	18.3
63.1	- 5.5	12.4	17.9
65.3	1.7	19.3	17.6
66.3	4.5	22.5	18.0
67.9	6.1	24.6	18.5
71.1	7.2	26.3	19.1
72.7	7.2	26.3	19.1
77.5	7.4	26.4	19.0

APPENDIX F

PHYSICAL PROPERTIES OF CORE TEST FLUID

TABLE F-1 PHYSICAL PROPERTIES OF CORE TEST FLUID

Temp. °C	Viscosity Poise	Density gm/ml
20.0	0.01589	0.7582
21.0	0.01555	0.7576
22.0	0.01524	0.7569
23.0	0.01494	0.7562
24.0	0.01468	0.7556
25.0	0.01440	0.7549
26.0	0.01414	0.7542
27.0	0.01388	0.7536
28.0	0.01362	0.7529
29.0	0.01337	0.7522
30.0	0.01337	0.7515

PREVIOUSLY PUBLISHED PAPERS

Colorado State University Hydrology Papers

- No. 34 "Statistical Discrimination of Change in Daily Runoff," by Andre J. Dumas and Hubert J. Morel-Seytoux, August 1969.
- No. 35 "Stochastic Process of Precipitation," by P. Todorovic and V. Yevjevich, September 1969.
- No. 36 "Suitability of the Upper Colorado River Basin for Precipitation Management," by Hiroshi Nakamichi and Hubert J. Morel-Seytoux, October 1969.
- No. 37 "Regional Discrimination of Change in Runoff," by Viboon Nimmannit and Hubert J. Morel-Seytoux, November 1969.
- No. 38 "Evaluation of the Effect of Impoundment on Water Quality in Cheney Reservoir," by J.C. Ward and S. Karaki, March 1970.
- No. 39 "The Kinematic Cascade as a Hydrologic Model," by David F. Kibler and David A. Woolhiser, February 1970.
- No. 40 "Application of Run-Lengths to Hydrologic Series," by Jaime Saldarriaga and Vujica Yevjevich, April 1970.
- No. 41 "Numerical Simulation of Dispersion in Groundwater Aquifers," by Donald Lee Reddell and Daniel K. Sunada, June 1970.
- No. 42 "Theoretical Probability Distributions for Flood Peaks," by Emir Zelenhasic, November 1970.
- No. 44 "Flood Routing Through Storm Drains, Part III, Evaluation of Geometric and Hydraulic Parameters," by V. Yevjevich and A.H. Barnes, November 1970.
- No. 45 "Flood Routing Through Storm Drains, Part II, Physical Facilities and Experiments," by V. Yevjevich and A.H. Barnes, November 1970.
- No. 46 "Flood Routing Through Storm Drains, Part III, Evaluation of Geometric and Hydraulic Parameters," by V. Yevjevich and A.H. Barnes, November 1970.
- No. 47 "Mathematical Simulation of Infiltrating Watersheds," by Roger E. Smith and David A. Woolhiser, January 1971.
- No. 48 "Models for Subsurface Drainage," W.E. Hedstrom, A.T. Corey and H.R. Duke, February 1971.